frontiers | Frontiers in Earth Science

TYPE Original Research
PUBLISHED 03 March 2025
DOI 10.3389/feart.2025.1532124

OPEN ACCESS

EDITED BY
Pengchun Li,
Chinese Academy of Sciences (CAS), China

REVIEWED BY
Weiliang Liu,
Sun Yat-sen University, China
Jian Xu,
Chinese Academy of Sciences (CAS), China

*CORRESPONDENCE
Hui Xie,
xiehuihaoba@163.com

RECEIVED 21 November 2024
ACCEPTED 11 February 2025
PUBLISHED 03 March 2025

CITATION
Xu J, Xie H, Luo Z, Chen Y and Shi H (2025) Geochronology and geochemistry of late Cenozoic volcanics on Naozhou Island, South China: insights into the interaction between the paleo-subduction slab and the Hainan mantle plume.
Front. Earth Sci. 13:1532124.
doi: 10.3389/feart.2025.1532124

Geochronology and geochemistry of late Cenozoic volcanics on Naozhou Island, South China: insights into the interaction between the paleo-subduction slab and the Hainan mantle plume

Jin Xu[1,2], Hui Xie[1,2,3,4]*, Zixuan Luo[1,2], Yanting Chen[1,2] and Hongcai Shi[1,2,3,4]

[1]Laboratory for Coastal Ocean Variation and Disaster Prediction, College of Ocean and Meteorology, Guangdong Ocean University, Zhanjiang, China, [2]Key Laboratory of Marine Mineral Resources, Ministry of Natural Resources, Guangzhou, China, [3]Key Laboratory of Climate, Resources and Environment in Continental Shelf Sea and Deep Sea of Department of Education of Guangdong Province, Guangdong Ocean University, Zhanjiang, China, [4]Key Laboratory of Space Ocean Remote Sensing and Application, Ministry of Natural Resources, Beijing, China

The mechanisms and processes of interaction between paleo-subducted slabs and mantle plumes are not well understood, primarily due to the challenges associated with direct observation. The Leiqiong Area (LQA), located in the northwestern South China Sea (SCS), may provide an ideal site to study the interaction between mantle plumes and paleo-subducted slabs. Extensive Late Cenozoic volcanic activities are present in the LQA, encompassing the Leizhou Peninsula (LP) and northern Hainan Island. This study conducted K-Ar dating, major and trace element analysis, and Sr-Nd-Pb-Hf isotopic analysis on volcanic rock samples from Naozhou Island, the largest volcanic island in the northeastern part of the LQA. The dating results show two periods of magmatic activities on Naozhou Island (3.6 Ma and 1 Ma). The geochemical results indicate that the columnar jointed basalts from Naozhou Island mainly show characters of oceanic island basalt (OIB). The isotopic data suggest origins of depleted MORB mantle (DMM) and Enriched Mantle II (EMII), with EMII potentially originating from the Hainan mantle plume. In view of these findings, the study further integrates data (Geochronology, trace elements and isotopic composition) from other volcanic rocks in the LQA to explore the deep mechanisms of extensive volcanic activity and plume-slab interactions along the northwestern SCS margin. We discovered that the volcanic rocks from southern LP and northern Hainan Island are characterized by OIB, IAB and OIB-IAB transition like, however, the volcanic rocks from Naozhou Island (northern LP) and Weizhou Island (western LP) are characterized by OIB like merely. This can be explained by a branched Hainan mantle plume model and may indicate the interaction between Hainan mantle plume and paleo-subdected slab mainly focuse on the center location of the plume rather than distal margin. This

conjecture is also in accord with the subduction direction of the Late Mesozoic subduction zone along the northern margin of the SCS.

KEYWORDS

South China sea, late Cenozoic, basaltic volcanics, Hainan mantle plume, Naozhou Island

1 Introduction

The interaction between mantle plumes and subducted slabs is a fundamental geodynamic process, exerting a significant influence on magmatic differentiation, volcanic edifice formation, and global geochemical fluxes (Foulger and Natland, 2003; Hofmann, 1997). The interaction may result in the flattening of subduction zones (Dalziel et al., 2000), the deflection of mantle plumes (Kincaid et al., 2013; Mériaux et al., 2015), extensive magmatic activity (Druken et al., 2014; Gazel et al., 2011; Yang et al., 2023), and compositional heterogeneity of mantle plumes (Xu et al., 2019; Xu et al., 2021; Yu et al., 2022), etc. Seismic tomography studies have revealed the presence of mantle plumes near certain subduction zones (Obrebski et al., 2010), suggesting potential interactions between mantle plumes and nearby subducting slabs (Mériaux et al., 2016; Toyokuni et al., 2022). Modern examples include the Tonga subduction zone and the Samoa plume (Price et al., 2014; Wendt et al., 1997; Chang et al., 2016), the Cascadia subduction zone and Yellowstone plume (Smith et al., 2009), as well as the Kamchatka subduction zone and the Kamchatka plume (Gorbatov et al., 2001). However, tomography has limitations in reconstructing slab-plume interactions from the pre-Cenozoic era. Evaluating pre-Cenozoic slab-plume interactions requires alternative proxies. Reconstructions of supercontinents and ancient large igneous provinces have demonstrated a spatiotemporal coupling between large igneous provinces and subduction abyssal systems (Wang et al., 2013), potentially indicating that slab-plume interactions were more widespread in ancient times. However, the processes by which subducted slabs are incorporated into mantle plumes and recycled back into the lithosphere remain unclear. The South China Sea (SCS), the largest marginal sea along the Western Pacific margin, has a complex tectonic history shaped by convergent and transform interactions among the Eurasian, Indo-Australian, and Pacific plates (Li et al., 2015; Li and Li, 2007; Briais et al., 2012; Taylor and Hayes, 1983) (Figure 1A). Its northern continental margin preserves a record of Late Mesozoic subduction history (Li et al., 2018; Cui et al., 2021), while the region is also characterized by the presence of the Hainan mantle plume (Xia et al., 2016) (Figure 1B). This makes the SCS a unique natural laboratory for studying interactions between mantle plumes and paleo-subducted slabs.

Late Cenozoic basaltic rocks are extensively distributed across the northwestern margin of the SCS, particularly in the Leiqiong Area (LQA), which encompasses the Leizhou Peninsula (LP) and northern Hainan Island, covering approximately 7,000 km^2. Previous studies have proposed three models to explain the magma sources and volcanic activities in the LQA. ① Sub-continental lithospheric mantle (SCLM) model. Tu et al. suggested that the late Cenozoic volcanism on Hainan Island originated from the SCLM, with magma generation primarily influenced by the dynamics of the lithospheric mantle beneath the region (Tu et al., 1991). Similarly, Zhu and Wang, and Huang et al. investigated the Quaternary volcanoes in the LQA, in terms of geochronology, whole-rock major and trace elements, and Sr-Nd-Pb isotopes, proposed that volcanic activity was controlled by fault activities, with magma primarily derived from the lithospheric mantle (Huang et al., 1993; Zhu and Wang, 1989). ② Mantle plume model. Plenty of researchers have suggested that the typical OIB-type basalts in the LQA were derived from Hainan mantle plume, a deep-seated upwelling of hot material from the lower mantle (Ho et al., 2000; Lei et al., 2009; Zou and Fan, 2010; Liu et al., 2015). ③ Mantle plume interacts with subducted slab model. Recent studies suggest that the magma source is a mixture of depleted MORB mantle (DMM) and Enriched Mantle II (EMII) components (Zhang et al., 2020; Yung-Tan et al., 2022; An et al., 2017), indicating the interaction between the Hainan mantle plume and subduction slab. Wang et al. proposed that the LQA represents a rare example of a young mantle plume interacting with a deeply subducted slab. They suggested that the volcanic activity on Hainan Island was influenced by subduction-related processes (Wang et al., 2012). Zhao et al. proposed that, based on whole-rock major and trace elements and olivine geochemistry, the volcanic rocks in the LP range from typical OIB-type to IAB-type, likely linked to the subduction of the Paleo-Pacific Plate (Zhao et al., 2021). Futhermore, Chen et al. employed *in situ* Sr isotope disequilibrium in plagioclases of late Cenozoic basalts to show the influence of recycled subduction-related H_2O-enriched oceanic fluids/melts carried by the deep Hainan mantle plume across the entire LQA (Chen et al., 2023).

As mentioned above, the magma sources of the volcanic rocks in the LQA remain controversial and the spatial distribution of the interaction between Hainan mantle plume and subducted slab are still unclear. Additionally, previous studies mainly focused on the region of southern LP and Hainan Island, sparsely research on the northern LP. Considering these volcanics on the northern LP are located in the distal margin of the Hainan mantle plume, therefore, their geochemical features and ages may provide some valuable constraints about the evolution and spatial pattern of the plume, even the plume-slab interaction.

This study collected 20 volcanic rock samples from Naozhou Island, the largest volcanic island in South China Sea (Figures 1C,D). Through detailed geochemical analyses of whole-rock major and trace elements, coupled with high-precision Sr-Nd-Pb-Hf isotope geochemistry and K-Ar geochronology. We aim to delineate the magmatic sources and temporal evolution of the Naozhou Island basalts and discuss the spatial distribution of magma sources in the LQA combined with previously published data. This work fills the gap in petrological and geochemical records in the northern LP, where volcanic rock detail data have been lacking. By providing new insights into this underexplored region, our work makes a

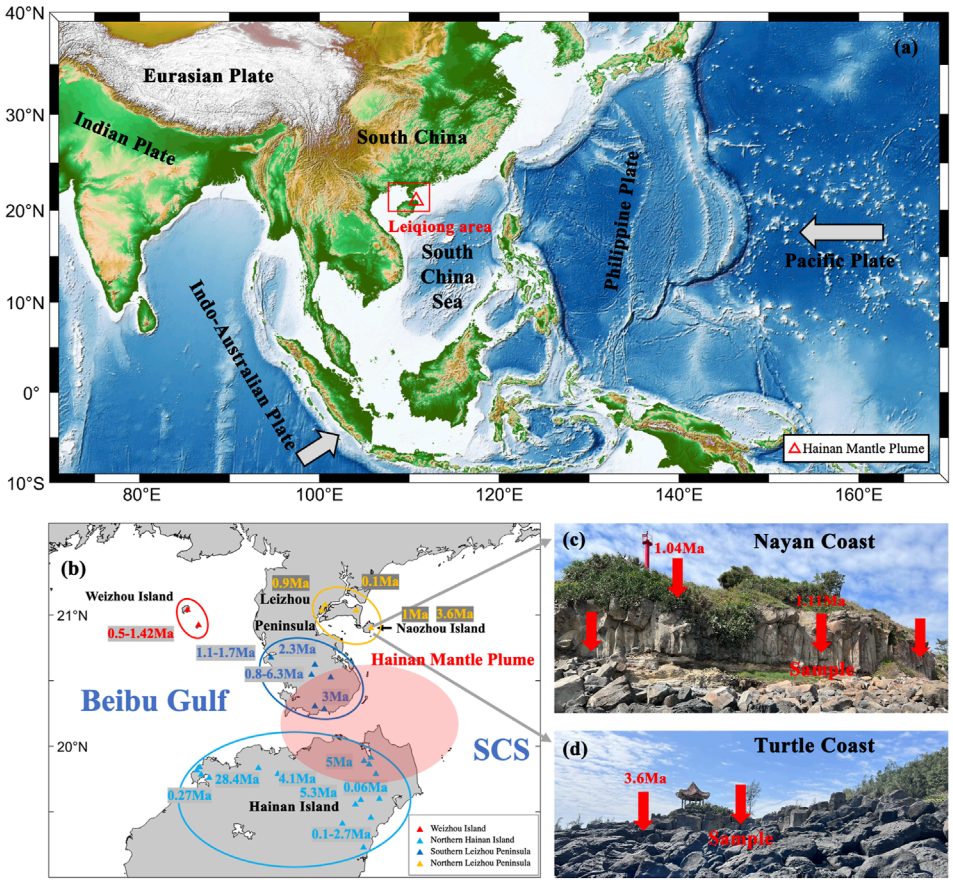

FIGURE 1
Map of the geological setting of the LQA. **(a)** Geological setting of the SCS (Briais et al., 2012; Taylor and Hayes, 1983); **(b)** Distribution of volcanoes ages in the LQA (Huang et al., 1993; Zhu and Wang, 1989; Zhang et al., 2020; Fan et al., 2006; Wang et al., 2021), Hainan Mantle Plume location (Xia et al., 2016); **(c)** Nayan Coast; **(d)** Turtle Coast.

complementary contribution to the comprehensive understanding of mantle dynamics and magmatic processes across the entire LQA. This work not only refines our understanding of magmatic origins and mantle dynamics in the northwestern SCS margin but also provides a framework for future studies investigating plume-slab interactions in analogous tectonic settings globally.

2 Geological background and sampling

The SCS is bordered by three major tectonic plates: the Eurasian Plate, the Indo-Australian Plate, and the Pacific Plate (Taylor and Hayes, 1983). The LQA, located on the northwestern margin of the SCS, is a region characterized by extensive late Cenozoic volcanism (Figure 1B) (Huang et al., 1993; Zhu and Wang, 1989; Zhang et al., 2020; Fan et al., 2006; Wang et al., 2021). The LQA is intersected by numerous faults trending in SE-NW and NE-SW directions, as documented by (Zhang and Zhao, 1984). The volcanic activities in this region span from the late Miocene to the Holocene, with a notable peak in the Quaternary period (Huang et al., 1993; Zhu and Wang, 1989; Zhang, 1990).

Naozhou Island, located in the northeastern part of the LQA, stands as the largest volcanic island in South China. It spans an area of approximately 56 km^2 and extends in a northeast-southwest direction. The island features a gently sloping topography. The highest point, 81.6 m above sea level, is in the east, and the elevation gradually descends towards the west. Naozhou Island is mainly composed of late Cenozoic basaltic lava flows. These lava flows are interbedded with tuffaceous layers and overlaid by unconsolidated Quaternary sediments. Notably, on the seaward side of the volcanic crater in the eastern part of the island, there are two well-developed sets of columnar joints on display (Figure 1).

A total of 20 fresh volcanic rock samples were collected from Naozhou Island. The volcanic rocks exhibit a porphyritic texture, with phenocrysts of olivine, pyroxene, and plagioclase as revealed in the thin sections. For example, the sample NZ-12 (Figure 2A) shows such a porphyritic feature with phenocryst accounting for 15% and matrix for 85% (volume percentage). The matrix consists mainly of acicular microcrystalline plagioclase interspersed with finer pyroxene and magnetite. The phenocrysts are dominated by subhedral olivine, pyroxene, and euhedral plagioclase.

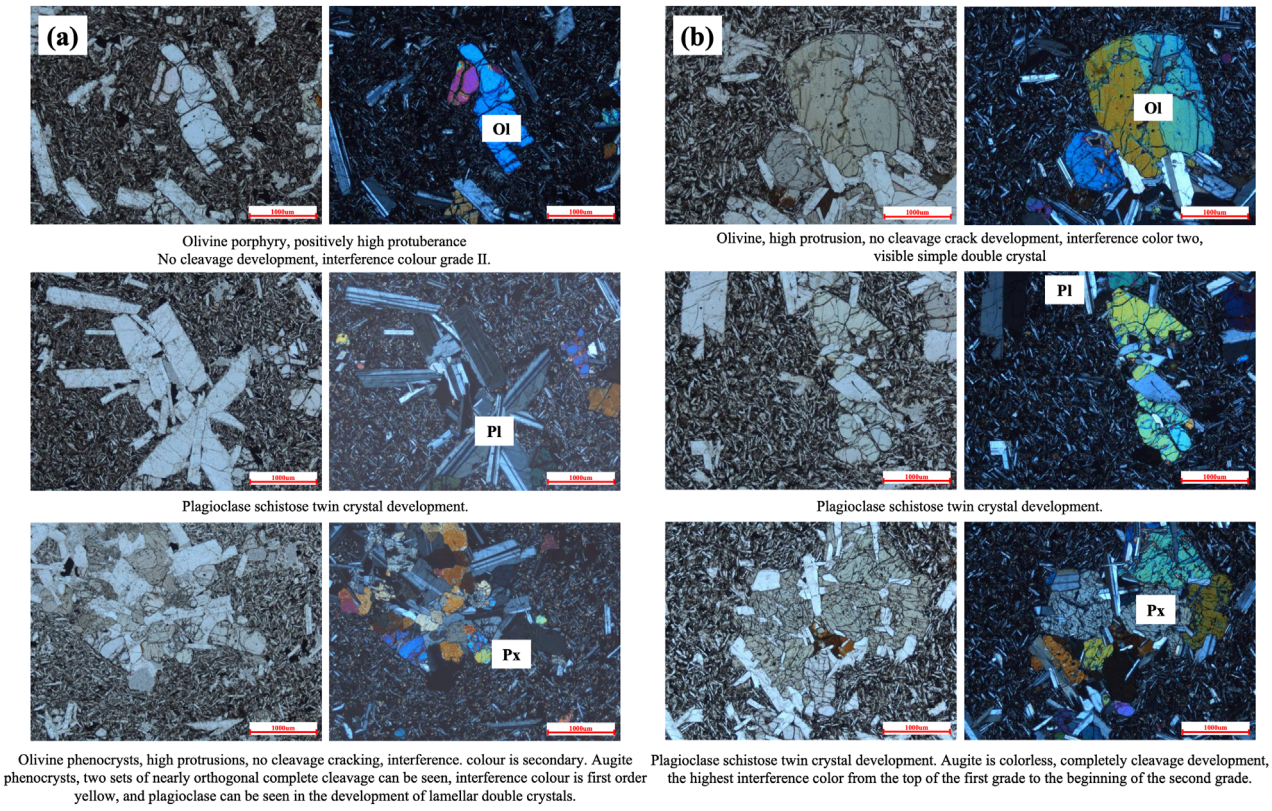

FIGURE 2
Olivine, clinopyroxene, and plagioclase phenocrysts of volcanic rock samples from Naozhou Island. **(a)** Sample NZ-12, **(b)** Sample NZ-28. Left: plane-polarised light; Right: orthogonal-polarised light.

TABLE 1 K-Ar dating results of volcanic rocks on the Naozhou Island.

Sample	Area	Lithology	K_2O (%)	$^{40}Ar_{rad}$ (g mol/g)	$^{40}Ar_{rad}$ (%)	Age (Ma)	±1σ
NZ-12	Turtle coast	Basaltic andesite	0.98	4.9E-12	2.18	3.6	0.05
NZ-22	Nayan coast	Basaltic andesite	1.14	1.76E-12	2.47	1.11	0.02
NZ-28	Nayan coast	Basaltic andesite	1.14	1.65E-12	4.98	1.04	0.02

[a]Ar_{rad}: Radioactive Ar.

3 Methods

3.1 K-Ar chronology

K-Ar dating was performed at the Analytical Laboratory of the Beijing Research Institute of Uranium Geology, China. Rock samples were crushed to 60 mesh, and porphyritic minerals were removed under a stereoscope. The samples were then cleaned using ultrasonic oscillation in alcohol, deionized water, and acetone, and subsequently divided into two portions.

One portion of the sample was precisely weighed (±0.001 mg) and wrapped in pure aluminum foil. The sample was then vacuum-baked for 48 h to remove adsorbed gases before being placed in a double-vacuum furnace for complete melting and gas extraction. The released gases were purified using a U-shaped liquid nitrogen cold trap and two zirconium-aluminum getter pumps operating at 450°C and room temperature, respectively. A known quantity of ^{38}Ar was introduced as a diluent, and the sample's Ar isotopic composition was analyzed using an Argus VI rare gas mass spectrometer. The analysis results were corrected for background, atmospheric Ar, and mass discrimination. The radiogenic $^{40}Ar^*$ content was calculated using the measured Ar isotope ratios and the known amount of ^{38}Ar diluent.

The second portion of the sample was weighed, and its K content was determined by atomic absorption spectrometry. The ^{40}K

10.3389/feart.2025.1532124

TABLE 2 Major element compositions of the Naozhou Island volcanic rocks (%).

	NZ-01	NZ-02	NZ-03	NZ-05	NZ-10	NZ-11	NZ-20	NZ-21	NZ-22	NZ-12
SiO_2	52.41	51.19	52.01	50.67	52.01	52.27	51.84	52.32	52.45	52.32
TiO_2	1.58	1.55	1.52	1.64	1.55	1.60	1.79	1.58	1.57	1.53
Al_2O_3	16.31	16.22	16.20	17.44	16.15	16.17	18.21	16.15	15.87	16.08
$^{T}Fe_2O_3$	8.78	8.91	8.92	9.61	9.11	9.09	7.90	9.05	8.90	8.43
MnO	0.11	0.10	0.10	0.12	0.11	0.11	0.09	0.12	0.11	0.13
MgO	5.40	5.50	5.77	5.68	6.08	5.81	3.60	5.99	5.91	5.68
CaO	8.73	8.70	8.58	8.82	8.60	8.54	9.31	8.50	8.53	9.22
Na_2O	3.66	3.58	3.62	3.54	3.57	3.58	3.94	3.51	3.50	3.27
K_2O	1.42	1.32	1.38	1.03	1.35	1.39	1.06	1.35	1.38	1.14
P_2O5	0.33	0.31	0.32	0.33	0.33	0.34	0.35	0.33	0.33	0.28
SO_3	0.00	0.01	0.01	0.01	0.08	0.06	0.07	0.01	0.04	0.27
LOI[a]	1.04	1.87	1.20	1.02	0.74	0.47	1.45	0.30	0.49	0.97
Total	99.75	99.23	99.62	99.90	99.67	99.41	99.59	99.20	99.07	99.34
	NZ-13	NZ-15	NZ-16	NZ-23	NZ-24	NZ-25	NZ-27	NZ-28	NZ-17	NZ-18
SiO_2	52.25	51.65	52.30	52.82	51.94	50.65	53.46	52.94	51.93	52.87
TiO_2	1.52	1.46	1.47	1.60	1.55	1.72	1.68	1.62	1.67	1.51
Al_2O_3	16.06	15.41	15.53	16.22	15.95	15.62	16.54	16.45	17.13	15.56
$^{T}Fe_2O_3$	9.00	10.04	8.86	8.11	8.75	10.31	7.70	8.54	8.80	9.28
MnO	0.13	0.15	0.12	0.11	0.13	0.12	0.10	0.16	0.11	0.13
MgO	6.32	5.38	6.65	5.09	5.66	6.60	4.48	5.33	4.62	6.70
CaO	9.05	8.68	8.73	8.75	8.55	9.04	8.94	8.85	7.55	8.79
Na_2O	3.24	3.06	3.14	3.59	3.55	3.52	3.49	3.56	3.04	2.98
K_2O	1.17	1.10	1.14	1.36	1.41	1.06	1.36	1.45	1.27	1.08
P_2O_5	0.28	0.26	0.27	0.33	0.33	0.31	0.35	0.35	0.30	0.27
SO_3	0.16	0.15	0.11	0.04	0.05	0.04	0.03	0.03	0.03	0.01
LOI	0.86	2.06	0.92	0.84	0.86	0.32	0.68	0.64	2.64	0.00
Total	100.03	99.40	99.23	98.85	98.73	99.28	98.80	99.90	99.09	99.17

[a]LOI: loss on ignition.

content was then derived from the measured K content, assuming a constant $^{40}K/K$ ratio within Earth's lithosphere. The ^{40}K-^{40}Ar age was calculated using the standard isotopic decay equation:

$$t = \frac{1}{\lambda} \ln \left[1 + \left(\frac{\lambda}{\lambda_e} \right) * \left({}^{40}Ar^* / {}^{40}K \right) \right]$$

Where λ is the total decay constant at ^{40}K (Potassium). The decay constant adopted the recommended value of 5.543 × 10^{-10} from Steiger and Jager (Steiger and Jäger, 1977). Standard substance adopts ZBH-25 black mica. Standard sample test results are included in the Supplementary Information.

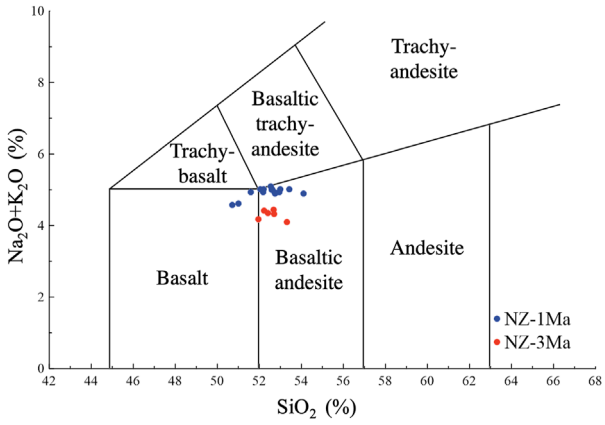

FIGURE 3
Total alkali-silica diagram of the Naozhou Island volcanic rocks. TAS grid is from Le Maitre et al. (2002).

3.2 Major and trace element

Major element analysis of whole-rock samples was performed using an Axios MAX XRF at Nanjing Hongchuang Geological Exploration Technology Service Co., Ltd. The procedure was as follows: (Foulger and Natland, 2003): Sample powders (200 mesh) were dried at 120°C for 8 h; (Hofmann, 1997); Approximately 0.5–1.0 g of dried sample was weighed in a constant-weight ceramic crucible and heated in a muffle furnace at 1,000°C for 200 min. The sample was then cooled to room temperature to calculate the loss on ignition (LOI); (Dalziel et al., 2000); A mixture of Canadian Claisse flux (6.0000 g ± 0.3 mg, 49.75% $Li_2B_4O_7$: 49.75% $LiBO_2$: 0.5% LiBr) and 0.6000 g ± 0.3 mg of dried sample was prepared and homogenized using a quartz rod. The mixture was transferred to a platinum crucible and melted at 1,100°C. After melting, the glass bead was cooled and prepared for XRF analysis.

Trace element analysis was conducted using an Elan DRC-e ICP-MS at Nanjing Hongchuang Geological Exploration Technology Service Co., Ltd. The sample digestion procedure was as follows: (Foulger and Natland, 2003): Sample powders (200 mesh) were dried at 105°C for 12 h; (Hofmann, 1997); 50 mg of dried sample was weighed and placed in a Teflon bomb; (Dalziel et al., 2000); 1.5 mL of HNO_3, 1.5 mL of HF, and 0.1 mL of $HClO_4$ (all ultrapure) were added to the Teflon bomb; (Kincaid et al., 2013); The Teflon bomb was sealed in a stainless steel pressure jacket and heated at 190°C for 48 h; (Mériaux et al., 2015); After cooling, the solution was evaporated to near dryness on a hotplate at 140°C, and then 3 mL of HNO_3 was added and evaporated again; (Druken et al., 2014); 3 mL of 50% HNO_3 was added, the bomb was resealed, and heated at 190°C for 12 h; (Gazel et al., 2011); The final solution was diluted to 100 g with Milli-Q water and spiked with 1 mL of a Rh + Re mixed standard solution (1 mg/L). Major elements were tested using GBW07104, GBW07105, GBW07310, GBW07312, GBW07314, and GBW07316 standards, while trace elements were tested using AGV-2 and BHVO-2 standards. Analytical precision was better than 3% for major elements and 1% for trace elements. Results of standard sample tests are included in the Supplementary Information.

3.3 Sr-Nd-Pb-Hf isotope

High-precision isotopic measurements (Sr, Nd, Hf, Pb) were conducted using a Nu Plasma II MC-ICP-MS at Nanjing Hongchuang Geological Exploration Technology Service Co., Ltd. (NHEXTS), Nanjing, China. Volcanic rock powders were digested in high-pressure PTFE bombs with 0.5 mL of 60% HNO_3 and 1.0 mL of 40% HF. The bombs were steel-jacketed and heated at 195°C for 3 days. The digested samples were then dried on a hotplate and reconstituted in 1.5 mL of 0.2 N HBr +0.5 N HNO_3 before ion exchange purification (N: Normality).

1. Pb Separation: Pb was separated using a Biorad AG1-X8 anion exchange column. Lithophile elements, Hf, Sr, and rare earth element (REEs) were washed out with 0.2 N HBr +0.5 N HNO_3, and Pb was eluted with Milli-Q water. Due to impurities, a second anion exchange column was used for further purification.
2. Hf, Sr, and REE Separation: A Biorad AG50W-X8 cation exchange column was used to roughly separate Hf, Sr, and REEs. After drying and re-dissolving the collected fraction in 1.5 N HCl, Hf was eluted with 1.5 N HCl, matrix elements with 2.0 N HCl, Sr with 2.5 N HCl, and REEs with 6.0 N HCl.
3. Hf Separation: Hf was separated from other high field strength elements (HFSE) using HDEHP-coated Teflon powder (LN-specific resin). After drying and re-dissolving the HFSE fraction in 3.0 N HCl, Hf was eluted with 2.0 N HF.
4. Sr Purification: The impure Sr fraction was further purified using Sr-specific resin after re-dissolution in 2.5 N HNO_3.
5. Nd Separation: REE fractions were further processed using Ln-specific resin. LREEs were removed with 0.12 N HCl, Nd was collected with 0.18 N HCl, and Sm with 0.4 N HCl.
6. Final Preparation: The Sr, Nd, Pb, and Hf fractions were evaporated to dryness and re-dissolved in 1.0 mL of 2% HNO_3. Elemental concentrations were measured using an Agilent 7,700x quadrupole ICP-MS. Diluted solutions were introduced into the Nu Plasma II MC-ICP-MS through a Teledyne Cetac Aridus II desolvating nebulizer.
7. Data Correction and Calibration: Isotopic ratios were corrected for mass fractionation using internal standards: $^{86}Sr/^{88}Sr$ = 0.1194 for Sr, $^{146}Nd/^{144}Nd$ = 0.7219 for Nd, $^{179}Hf/^{177}Hf$ = 0.7325 for Hf, $^{205}TL/^{203}TL$ = 2.3885 for Pb. Instrumental drift was monitored using international isotopic standards (NIST SRM 987 for Sr, JNdi-1 for Nd, Alfa Hf, and NIST SRM 981 for Pb).

Geochemical reference materials (USGS BCR-2, BHVO-2, AVG-2, RGM-2) were used for quality control, with results agreeing with previous publications within analytical uncertainty (Weis et al., 2007; Weis et al., 2006). Detailed results of standard sample tests are provided in the Supplementary Information.

4 Results

4.1 K-Ar chronology

This work performed K-Ar dating results for three volcanic rock samples from Naozhou Island, which reveal

10.3389/feart.2025.1532124

TABLE 3 Trace and rare earth element compositions of the Naozhou Island volcanic rocks (ppm).

	NZ-01	NZ-02	NZ-03	NZ-05	NZ-10	NZ-11	NZ-20	NZ-21	NZ-22	NZ-12
Li	5.78	7.01	6.76	9.74	5.13	5.18	6.84	6.19	5.66	4.11
Be	1.67	1.41	1.54	1.27	1.36	1.44	1.19	1.65	1.68	1.28
Sc	18.55	18.73	18.75	19.04	16.14	16.90	20.33	17.72	15.75	16.38
V	139.32	138.21	136.93	145.75	143.92	145.91	163.08	160.62	161.74	148.43
Cr	192.12	200.27	203.97	202.87	239.09	203.81	272.70	216.10	216.45	276.78
Co	32.66	34.20	34.33	34.38	37.36	36.87	21.96	39.38	38.34	41.38
Ni	79.90	90.47	89.34	86.85	1.15	0.13	85.50	9.59	0.52	1.16
Cu	72.93	58.82	64.31	49.32	63.85	68.56	80.16	74.21	73.03	67.22
Zn	83.97	83.73	106.02	90.42	80.12	83.38	97.84	103.94	104.16	82.95
Ga	19.87	19.76	19.72	20.95	19.04	19.92	22.43	22.16	21.71	19.21
Rb	25.67	15.53	26.49	8.01	21.46	23.57	8.07	23.00	22.27	26.52
Sr	489.26	471.64	484.92	508.14	521.24	540.50	592.01	538.02	528.31	515.58
Y	15.43	14.88	14.97	16.62	15.48	16.81	19.68	16.67	16.34	18.54
Zr	123.23	123.86	119.80	128.38	121.78	131.80	146.11	138.75	138.13	116.07
Nb	28.32	26.63	27.95	29.46	28.86	30.75	28.48	29.32	29.19	23.93
Cs	0.21	0.36	0.48	0.06	0.19	0.16	0.08	0.13	0.16	0.59
Ba	257.73	256.11	250.79	324.13	256.54	276.02	360.46	281.81	279.39	228.22
La	19.25	19.19	18.01	20.31	19.01	20.68	23.85	19.76	19.44	16.61
Ce	36.84	36.78	33.98	35.67	35.41	38.45	41.24	39.30	38.70	32.10
Pr	4.38	4.38	4.12	4.62	4.30	4.71	5.32	4.94	4.86	4.00
Nd	18.09	18.14	16.94	19.11	17.17	18.53	23.17	19.56	19.36	16.54
Sm	4.26	4.27	3.99	4.47	4.05	4.40	5.08	4.60	4.52	4.08
Eu	1.51	1.52	1.41	1.59	1.31	1.41	1.84	1.63	1.61	1.32
Gd	4.06	4.10	3.79	4.25	3.76	4.08	5.11	4.55	4.48	3.94
Tb	0.60	0.61	0.56	0.62	0.57	0.63	0.77	0.61	0.61	0.62
Dy	3.23	3.30	2.99	3.34	3.26	3.48	4.14	3.41	3.37	3.56
Ho	0.60	0.61	0.55	0.61	0.61	0.65	0.72	0.66	0.65	0.68
Er	1.45	1.50	1.36	1.50	1.41	1.51	1.86	1.50	1.46	1.60
Tm	0.20	0.20	0.18	0.20	0.19	0.21	0.24	0.21	0.20	0.22
Yb	1.15	1.19	1.05	1.17	1.07	1.16	1.42	1.24	1.21	1.23
Lu	0.17	0.17	0.15	0.16	0.16	0.17	0.21	0.17	0.17	0.18
Hf	2.98	3.03	2.73	2.96	2.85	3.04	3.79	3.29	3.30	2.79

(Continued on the following page)

10.3389/feart.2025.1532124

TABLE 3 (*Continued*) Trace and rare earth element compositions of the Naozhou Island volcanic rocks (ppm).

	NZ-01	NZ-02	NZ-03	NZ-05	NZ-10	NZ-11	NZ-20	NZ-21	NZ-22	NZ-12
Ta	1.61	1.65	1.49	1.62	1.58	1.68	1.75	1.98	1.98	1.32
Tl	0.040	0.030	0.031	0.007	0.030	0.031	0.018	0.042	0.041	0.065
Pb	2.82	2.73	3.94	2.70	2.62	2.76	2.96	2.96	2.91	7.52
Th	3.35	3.42	2.97	3.21	3.00	3.29	3.60	3.29	3.22	2.77
U	0.73	0.62	0.65	0.49	0.62	0.67	0.71	0.74	0.68	0.73
	NZ-13	NZ-15	NZ-16	NZ-23	NZ-24	NZ-25	NZ-27	NZ-28	NZ-17	NZ-18
Li	5.19	3.99	5.56	6.02	5.73	5.61	4.32	5.04	55.38	5.77
Be	1.23	1.22	1.09	1.63	1.61	0.97	1.53	1.32	1.43	1.08
Sc	14.29	20.73	13.75	15.54	17.90	20.16	18.45	15.35	18.80	20.60
V	140.95	147.77	152.65	161.76	152.50	225.22	157.56	152.13	167.51	157.35
Cr	245.32	351.45	260.45	217.37	216.58	282.99	221.97	202.81	357.10	271.42
Co	35.69	48.14	38.10	39.51	37.89	43.69	37.74	36.85	44.41	41.17
Ni	0.23	83.42	89.58	18.49	18.86	84.95	<0.000	<0.000	81.90	18.10
Cu	67.05	76.23	81.69	50.78	59.27	75.96	69.98	88.92	100.85	83.67
Zn	75.97	86.30	87.10	103.40	101.26	104.09	105.58	94.08	103.33	86.67
Ga	17.92	19.85	17.91	21.93	21.69	19.16	20.52	19.62	20.49	19.53
Rb	25.96	25.87	22.91	17.46	28.00	14.95	21.36	25.83	16.69	23.93
Sr	480.58	497.46	437.92	544.42	521.48	416.51	531.00	513.26	372.87	433.78
Y	16.10	19.80	13.96	16.83	16.21	17.53	17.14	14.93	18.42	15.62
Zr	111.96	113.41	113.30	138.87	135.67	107.83	141.52	134.91	132.72	116.38
Nb	22.95	23.16	19.38	29.74	28.53	18.38	27.76	26.42	24.06	18.75
Cs	0.54	0.54	0.56	0.31	0.30	0.14	0.44	0.49	0.28	0.61
Ba	219.26	229.60	219.94	284.75	267.76	214.20	372.69	289.05	304.69	224.54
La	15.67	17.74	14.53	19.78	18.95	15.23	21.10	19.56	18.36	15.49
Ce	30.56	32.84	28.56	39.63	37.49	29.25	38.67	36.14	32.43	29.69
Pr	3.80	4.06	3.56	4.96	4.75	3.88	4.83	4.53	4.30	3.74
Nd	15.55	16.79	15.93	19.76	18.63	17.76	21.40	19.74	19.21	16.76
Sm	3.87	4.14	3.73	4.60	4.37	4.19	4.71	4.41	4.39	3.96
Eu	1.24	1.33	1.35	1.64	1.56	1.47	1.68	1.53	1.60	1.43
Gd	3.69	4.05	3.74	4.55	4.31	4.34	4.64	4.24	4.45	4.03
Tb	0.58	0.63	0.59	0.62	0.59	0.70	0.70	0.65	0.70	0.63
Dy	3.32	3.70	3.23	3.44	3.26	3.91	3.75	3.42	3.80	3.47
Ho	0.63	0.71	0.56	0.66	0.63	0.70	0.65	0.59	0.67	0.61

(Continued on the following page)

TABLE 3 (*Continued*) Trace and rare earth element compositions of the Naozhou Island volcanic rocks (ppm).

	NZ-13	NZ-15	NZ-16	NZ-23	NZ-24	NZ-25	NZ-27	NZ-28	NZ-17	NZ-18
Er	1.46	1.67	1.46	1.50	1.43	1.83	1.69	1.54	1.75	1.60
Tm	0.20	0.23	0.19	0.21	0.20	0.24	0.22	0.20	0.23	0.21
Yb	1.15	1.27	1.15	1.24	1.18	1.44	1.29	1.19	1.37	1.26
Lu	0.17	0.18	0.17	0.18	0.17	0.21	0.19	0.18	0.20	0.19
Hf	2.69	2.72	2.98	3.31	3.11	3.07	3.61	3.44	3.44	3.09
Ta	1.26	1.27	1.17	2.01	1.94	1.17	1.67	1.56	1.46	1.14
Tl	0.066	0.074	0.055	0.035	0.050	0.022	0.053	0.062	0.035	0.062
Pb	2.81	2.92	5.24	6.55	2.97	2.10	2.77	2.72	2.69	2.54
Th	2.55	2.77	2.48	3.26	3.16	2.20	3.33	3.14	3.07	2.67
U	0.63	0.62	0.57	0.70	0.70	0.67	0.72	0.76	0.78	0.58

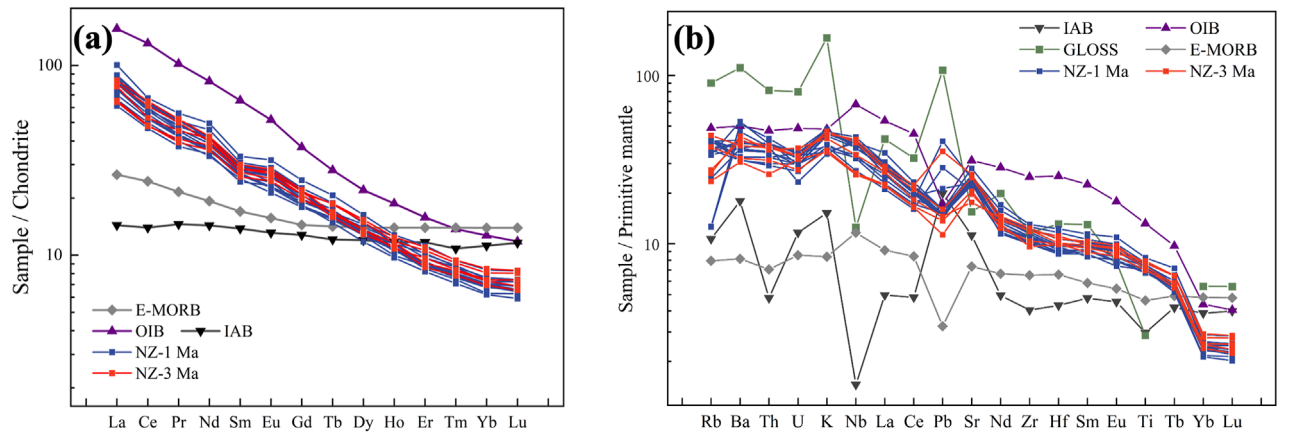

FIGURE 4
(a) Chondrite-normalized REE diagrams. Data for chondrites, OIBs, E-MORBs are from Sun et al. (1989). Data for IABs are from Niu and O'Hara (2003); **(b)** Primitive mantle-normalized trace element diagrams. Data for primitive mantle, OIBs, E-MORBs are from Sun et al. (1989). Data for IABs are from Niu and O'Hara (2003). Data for GLOSS are from Plank and Langmuir (1998).

two distinct periods of volcanic activity. The analytical data are listed in Table 1. On the Nayan Coast, to east of the volcanic crater, the age of upper part of the strata is 1.04 Ma (NZ-28), while the age of lower part is 1.11 Ma (NZ-22) (Figure 1C). On the Turtle Coast, to the southwest of the crater at a relatively lower elevation, sample NZ-12 was dated at 3.6 Ma (Figure 1D). These results suggest that volcanic activity on Naozhou Island occurred from the late Pliocene to the Pleistocene.

The columnar joints observed on Naozhou Island serve as clear indicator of magma solidification process. The ages obtained from these joints provide reliable constraints on the timing of volcanic eruption cycles. Our findings corroborate the stratigraphic contact relationships observed in the field (Wang et al., 2023). Based on these results, it can be inferred that magmatic activity on Naozhou Island occurred at least two periods: about 3.6 Ma and 1 Ma (1.11–1.04 Ma).

4.2 Major elements

The major element data are summarized in Table 2. SiO_2 content ranges from 50.2 to 54.11 wt%, TiO_2 from 1.46 to 1.8 wt%, Al_2O_3 from 15.32 to 18.13 wt%, total Fe_2O_3 ($^{T}Fe_2O_3$) from 7.8 to 10.38 wt%, MgO from 3.61 to 6.75 wt%, Na_2O from 2.85 to 3.95 wt%, K_2O from 1.03 to 1.45 wt%, and Mg# from 47.44 to 59.8. The loss on ignition (LOI) values are generally low, less than 2 wt% (Table 2). In the total alkali-silica (TAS) diagram (Figure 3) (Le Maitre et al., 2002), these volcanic rocks classified as basalt and basaltic andesite. The 1 Ma volcanic rocks have higher

10.3389/feart.2025.1532124

TABLE 4 Sr-Nd-Pb-Hf isotope results of volcanic rocks from the Naozhou Island.

Sample	$^{87}Sr/^{86}Sr$	2σ	$^{143}Nd/^{144}Nd$	2σ	$^{176}Hf/^{177}Hf$	2σ
NZ-1	0.703757	0.000013	0.512896	0.000012	0.283072	0.000007
NZ-2	0.703878	0.000014	0.512882	0.000013	0.283054	0.000005
NZ-10	0.703764	0.000010	0.512792	0.000016	-	-
NZ-11	0.703733	0.000008	0.512830	0.000018	-	-
NZ-12	0.704173	0.000010	0.512788	0.000016	0.283076	0.000006
NZ-13	0.703746	0.000013	0.512896	0.000008	0.283076	0.000006
NZ-21	0.703747	0.000012	0.512835	0.000016	-	-
NZ-22	0.703764	0.000010	0.512822	0.000018	0.283086	0.000006
NZ-28	0.703755	0.000016	0.512802	0.000018	-	-
Sample	$^{206}Pb/^{204}Pb$	2σ	$^{207}Pb/^{204}Pb$	2σ	$^{208}Pb/^{204}Pb$	2σ
NZ-1	18.672847	0.001078	15.647043	0.000970	39.006286	0.003208
NZ-2	18.655040	0.000872	15.649815	0.000756	39.028549	0.002089
NZ-10	18.616720	0.000472	15.630390	0.000400	38.876240	0.001266
NZ-11	18.577210	0.000488	15.628410	0.000416	38.832660	0.001260
NZ-12	18.437220	0.000522	15.701080	0.000464	38.666350	0.001456
NZ-13	18.638660	0.000865	15.638792	0.000732	38.898419	0.001981
NZ-21	18.612230	0.000496	15.631480	0.000400	38.877150	0.001204
NZ-22	18.592390	0.000514	15.631120	0.000434	38.851440	0.001426
NZ-28	18.600470	0.000496	15.638890	0.000448	38.871430	0.001504

alkalinity, with combined $Na_2O + K_2O$ values around 5%, while the 3.6 Ma volcanic rocks have values closer to 4%.

The TAS diagram shows that most of the 3 Ma rocks fall within the basaltic andesite field, indicating that these magmas were relatively more evolved, with moderate SiO_2 content and lower alkalinity. The 3 Ma samples show similar SiO_2 contents with those of 1 Ma samples. Some of the 1 Ma samples fall into the basalt field and exhibit higher $Na_2O+ K_2O$ values, indicating a trend toward higher alkalinity. Overall, the TAS diagram illustrates a clear distinction between the 3 Ma and 1 Ma volcanic rocks, with the latter showing evidence of higher alkalinity.

4.3 Trace elements

Despite two distinct periods of volcanic activity, the trace element patterns of these samples show no signifcant differences, indicating a stable mantle source over time (Table 3).

The total REE contents (ΣREEs) of the samples range from 92.71 to 134.66 ppm, with a mean of 111.13 ppm, which is lower than the typical OIB average of 198.9 ppm (Sun et al., 1989). In the chondrite-normalized REE diagram (Figure 4) (Sun et al., 1989; Niu and O'Hara, 2003; Plank and Langmuir, 1998), these volcanic rocks exhibit a clear enrichment in light REEs (LREEs), with $(La/Yb)_N$ values ranging from 7.58 to 12.79, averaged at 10.98. The Eu anomalies (Eu/Eu^*) range from 0.98 to 1.10, with a mean of 1.06, indicating minimal Eu anomalies. The slight enrichment in Eu relative to typical OIB values may reflect a weak influence of fractional crystallization, particularly involving plagioclase. The REE distribution patterns resemble the typical OIB.

The trace elements, patterns are also consistent with OIB, are featured by enrichment in large-ion lithophile elements (LILEs, such as Ba) and LREEs. Moreover, a few samples show a positive Pb anomaly. No significant negative Nb anomaly and U anomaly display in our samples.

Overall, the trace element and REE patterns observed in the Naozhou Island volcanic rocks suggest a mantle source that has remained stable across different volcanic episodes. The geochemical signatures are consistent with those of typical OIBs, indicating a mantle source enriched in LREEs and showing typical trace element behaviors associated with OIBs.

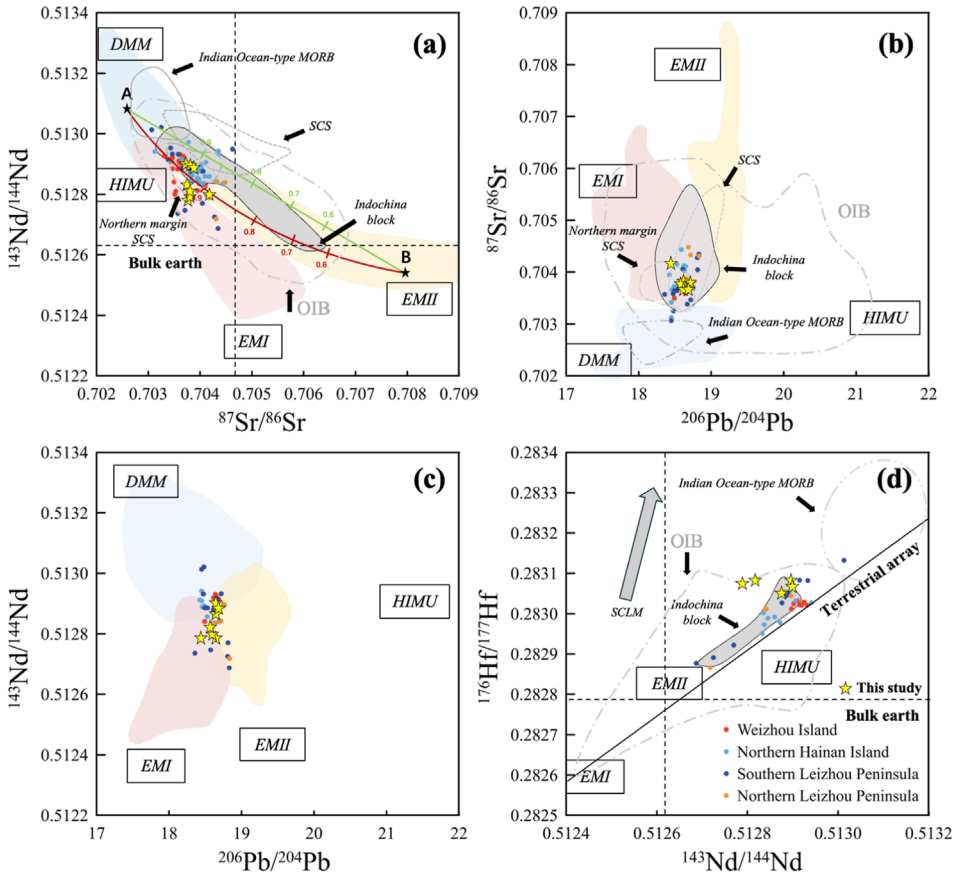

FIGURE 5
Sr-Nd-Pb-Hf isotope diagrams. **(a)** $^{143}Nd/^{144}Nd$ vs $^{87}Sr/^{86}Sr$ **(b)** $^{87}Sr/^{86}Sr$ vs $^{206}Pb/^{204}Pb$, **(c)** $^{143}Nd/^{144}Nd$ vs $^{206}Pb/^{204}Pb$, **(d)** $^{176}Hf/^{177}Hf$ vs $^{143}Nd/^{144}Nd$. Combined with data from the northern Leizhou Peninsula (This study and Zhao et al. (2021)), southern Leizhou Peninsula (Huang et al., 1993; Zhu and Wang, 1989; Zhao et al., 2021), Weizhou Island (Zhang et al., 2020; Fan et al., 2008; Li et al., 2014), and northern Hainan Island (Huang et al., 1993; Zhu and Wang, 1989; Wang et al., 2012; Zhao et al., 2021). The Naozhou Island data are included in the Northern Leizhou Peninsula. DMM, EMI, EMII and HIMU end-member (Zindler and Hart, 1986), Shaded areas representing end-members are from the data set (www.earthchem.org). OIBs end-member (Staudigel et al., 1984). SCS data (Yan et al., 2008; Yan et al., 2014; Yan et al., 2015). Northern margin SCS data (Tu et al., 1991; Zou and Fan, 2010; Zou et al., 2000). Indochina block data (An et al., 2017; Hoàng et al., 2013; Hoang et al., 1996). Indian ocean-type MORB end-member (Mahoney et al., 2012).

4.4 Sr-Nd-Pb-Hf isotopes

The Sr-Nd-Pb-Hf isotope ratios for the Naozhou Island volcanic rock samples are as follows (Table 4): $^{87}Sr/^{86}Sr$ = 0.703733–0.704173, $^{143}Nd/^{144}Nd$ = 0.512788–0.512896, $^{206}Pb/^{204}Pb$ = 18.43722–18.672847, $^{207}Pb/^{204}Pb$ = 15.62841–15.70108, $^{208}Pb/^{204}Pb$ = 38.66635–39.028549, and $^{176}Hf/^{177}Hf$ = 0.283054–0.283086. These isotope ratios are characteristic of OIB-type compositions (Figure 5).

In the $^{207}Pb/^{204}Pb$ and $^{208}Pb/^{204}Pb$ vs $^{206}Pb/^{204}Pb$ diagrams (Figure 6), the Naozhou Island samples plot above the Northern Hemisphere Reference Line (NHRL), resembling the Dupal anomaly observed in the Southern Hemisphere (Tu et al., 1991; Hart, 1984; Flower et al., 1992). The Dupal anomaly typically indicates the presence of EMII in the mantle source, and the position above the NHRL suggests that these rocks contain components that are more enriched than those from a DMM.

5 Discussion

5.1 Geochemical insights into crustal contamination and magmatic sources

5.1.1 Crustal contamination and fractional crystallization on Naozhou Island

Evaluating whether the magma experienced crustal contamination during its ascent is crucial for accurately determining the magma source and understanding the magma evolution process (Xu et al., 2005; Dai et al., 2018; Zeng et al., 2013; Wang et al., 2019). Nb/U and Ce/Pb ratios are sensitive indicators of crustal contamination, as crustal material typically lowers these ratios. The geochemical data of volcanic rocks from Naozhou Island exhibit primitive Nb/U ratios (30.88–60.21, average: 39.87) and Ce/Pb ratios (4.2–14, average: 11.6). These ratios are significantly higher than those typical of continental crust (Nb/U ≈ 6.15, Ce/Pb ≈ 3.91), suggesting that the magma was not significantly contaminated by crust (Rudnick and Gao, 2003; Salters and Stracke, 2004). The

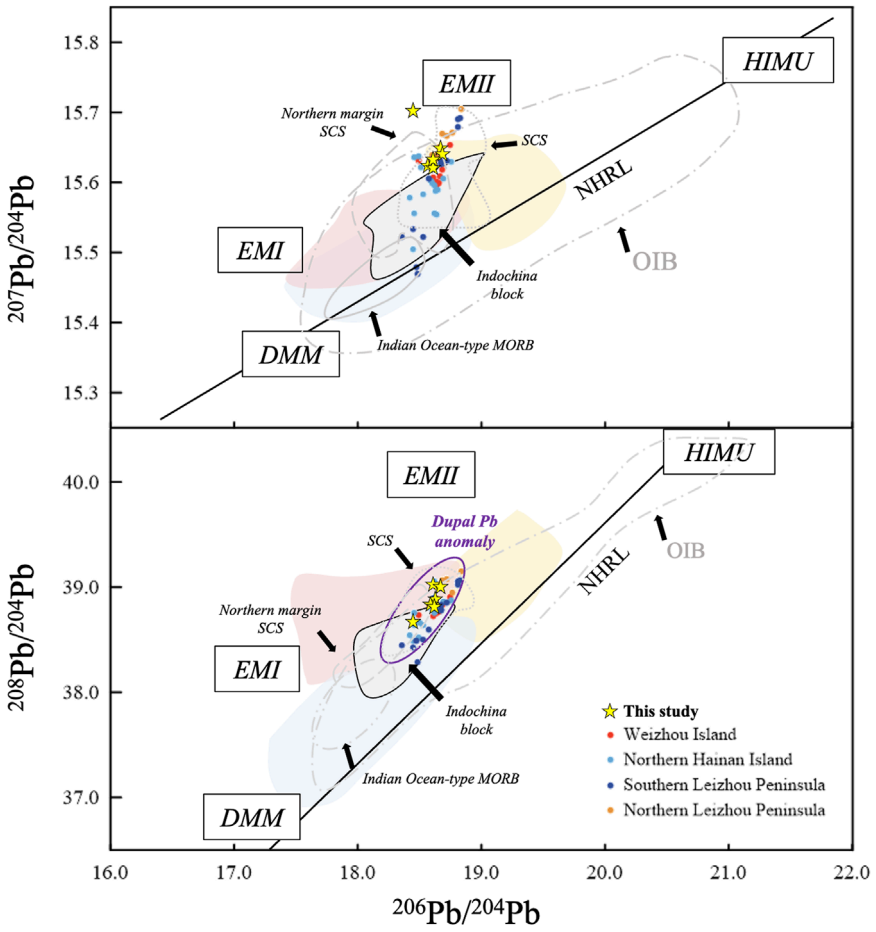

FIGURE 6
$^{207}Pb/^{204}Pb$ and $^{208}Pb/^{204}Pb$ vs $^{206}Pb/^{204}Pb$ isotope diagrams. The Dupal anomaly is from Dupré and Allègre (1983). The NHRL is North Hemisphere reference line (Hart, 1984).

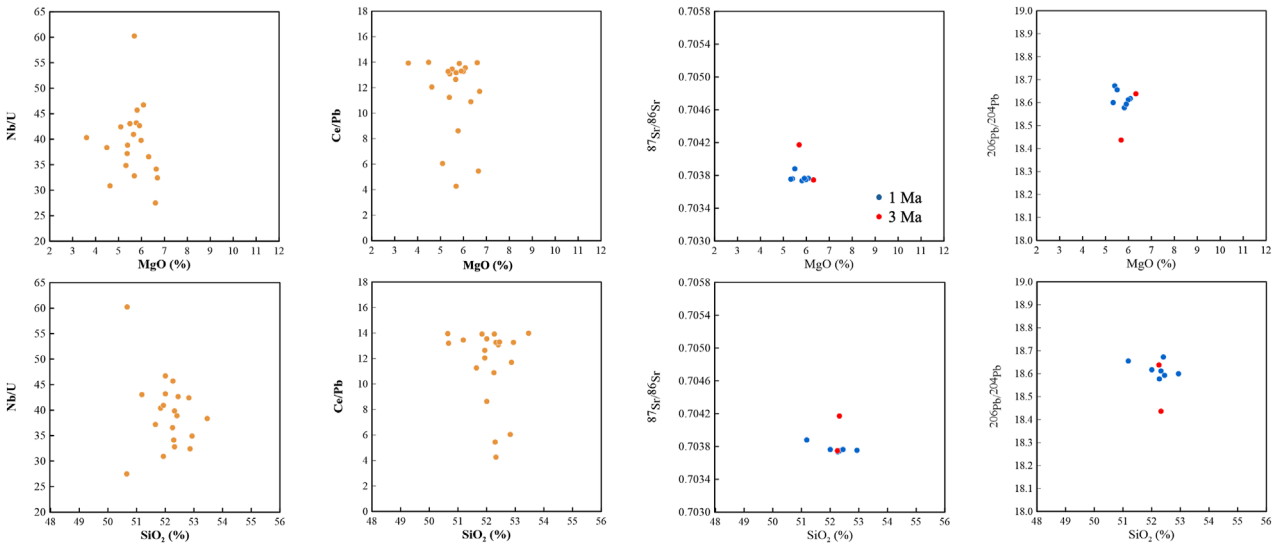

FIGURE 7
Correlations between trace element ratios (Nb/U, Ce/Pb) and isotopic ratios ($^{87}Sr/^{86}Sr$, $^{206}Pb/^{204}Pb$) with MgO and SiO_2.

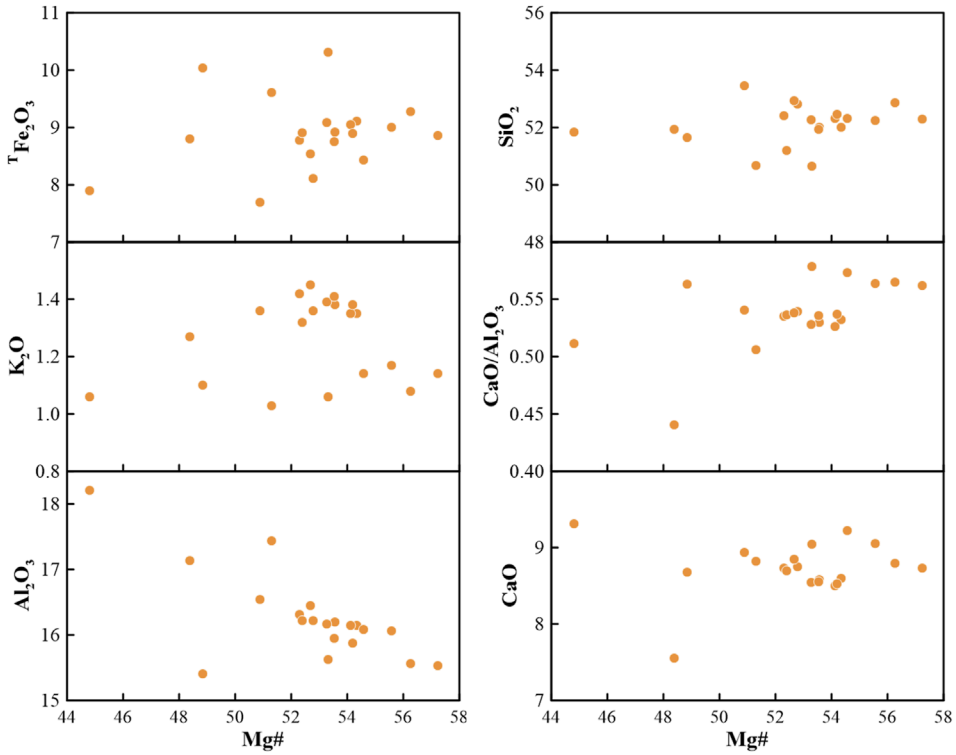

FIGURE 8
Variations in selected major-element oxides of Naozhou Island volcanic rocks.

absence of negative Nb anomalies in the trace element diagrams also suggests minimal crustal contamination (Figure 4). Furthermore, the ratios of sensitive elements (Nb/U, Ce/Pb) and isotopic data ($^{87}Sr/^{86}Sr$, $^{206}Pb/^{204}Pb$) are plotted against the contents of MgO and SiO_2 (Figure 7). The results demonstrate that there are no systematic trends of variation in these relationships, providing evidence that the influence of crustal contamination is limited (Zhang et al., 2020; Yan et al., 2018).

Fractional crystallization represents a crucial process in the evolution of magma. The Naozhou Island volcanic rocks exhibit Mg# contents ranging from 44.8 to 57.2 and Cr contents spanning from 192 to 357 ppm. These values are lower than those of primitive basalts (Mg# value >70, Cr contents >1,000 ppm) (An et al., 2017; Wilkinson and Maitre, 1987), which clearly indicates that these volcanic rocks have experienced fractional crystallization. Mg# displays a positive correlation with $^{T}Fe_2O_3$, SiO_2, and CaO/Al_2O_3, a negative correlation with K_2O and Al_2O_3, and no significant correlation with CaO (Figure 8). This pattern implies an evolutionary sequence of fractional crystallization, starting with the early crystallization of Olivine and pyroxenes and then transitioning to a medium stage dominated by plagioclase.

5.1.2 Magmatic source characteristics on Naozhou Island

Given that fractional crystallization does not alter the isotopic composition of magma (Staudigel et al., 1984; Hamelin and Allègre, 1985), the isotopic ratios thus can be used to indicate the characteristics of their magma source. The volcanic rocks' isotopic ratios can be used to infer the characteristics of their magma source. The Sr-Nd-Pb-Hf isotope data of volcanic rocks from Naozhou Island, showing between DMM and EMII reference values (Figure 5). Combined with those from adjacent regions (Zou and Fan, 2010; Zhang et al., 2020; Wang et al., 2012; Zhao et al., 2021; Yan et al., 2008; Yan et al., 2014), may suggest that basalt can be explained by a binary mixed model involving DMM and EMII endmember components. The DMM endmember represents a depleted mantle source, likely originating from the Indian MORB mantle, which is prevalent in late Cenozoic intraplate volcanism across Southeast Asia (An et al., 2017; Yan et al., 2018; Hoàng et al., 2013; Hoang et al., 1996). The EMII endmember is characterized by high $^{87}Sr/^{86}Sr$ (>0.705), low $^{143}Nd/^{144}Nd$ ratios (<0.5125) (Figure 5), and high Pb isotopic ratios ($^{206}Pb/^{204}Pb$ = 18.5–19.5) (Figure 6), they are usually associated with recycled continental or oceanic crust and sediments (von Huene et al., 2004; Wang et al., 2018). Previous studies have suggested that EMII in this region could originate from the SCLM or a mantle plume (Zhang et al., 2020; An et al., 2017; Yan et al., 2018; Yan et al., 2014; Yan et al., 2015).

The geochemical data from Naozhou Island suggest that the EMII corresponds to the mantle plume (Figure 5). The lithospheric mantle exhibits significant Nd-Hf isotopic decoupling due to fluid-driven metasomatism (Choi and Mukasa, 2012). The volcanic rocks on Naozhou Island exhibit the same linear array as those in the surrounding areas (Zhang et al., 2020; An et al., 2017; Yan et al., 2018; Yan et al., 2015) (Figure 5D). This indicates that EMII is more likely to originate from a mantle plume rather than SCLM. Secondly, the Nd-Hf isotopic composition of the SCLM is typically different

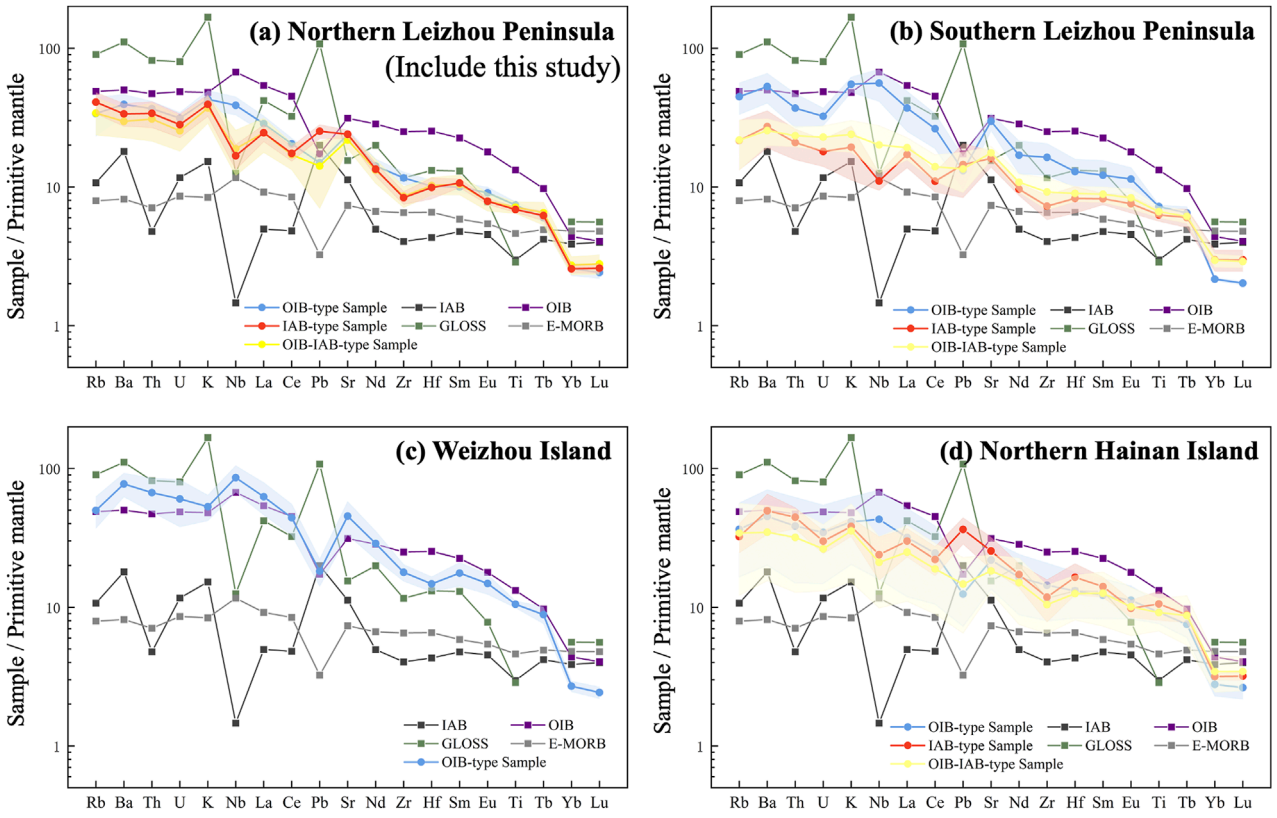

FIGURE 9
Primitive mantle-normalized trace element diagrams. **(a)** Northern Leizhou Peninsula (including this study), **(b)** Southern Leizhou Peninsula, **(c)** Weizhou Island, **(d)** Northern Hainan Island. Lines integrated from regional data average and the shadows were fields ranges. Weizhou Island data (Zhang et al., 2020; Fan et al., 2008); Leizhou Peninsula and Northern Hainan Island data (Ho et al., 2000; Liu et al., 2015; Yung-Tan et al., 2022; Wang et al., 2012; Zhao et al., 2021). Lines integrated from regional data average and the shadows were fields ranges.

from that of oceanic island basalts. The samples from Naozhou Island all fall within the OIB range (Figure 5D), further ruling out the influence of the SCLM. Additionally, SCLM often shows more enriched Sr isotopic signatures, which are not observed in Naozhou Island. Based on seismic tomography studies, a low-velocity conduit extending from the lower mantle to the shallow lithosphere has been identified, indicating the presence of the Hainan mantle plume in the region (Figure 1B) (Toyokuni et al., 2022; Xia et al., 2016; Lei et al., 2009; Lebedev and Nolet, 2003; Chen et al., 2021; Hua et al., 2022). In summary, geochemical and geophysical evidence suggests that the EMII endmember in Naozhou Island may originate from the Hainan mantle plume, consistent with findings from surrounding areas (Figures 5, 6, 9).

5.2 Temporal evolution of volcanic activities in the Leiqiong Area

This study conducted K-Ar dating revealing two major periods of volcanic activity on Naozhou Island: approximately 3.6 Ma (late Pliocene) and 1 Ma (Pleistocene). These K-Ar dating results provide a reliable framework for understanding the timing of volcanism Naozhou Island. The volcanic rock ages across the LQA (Table 5; Figure 10A) reveals that the volcanic activities period predominantly occurred during the Quaternary period (Huang et al., 1993; Zhu and Wang, 1989; Zhang et al., 2020; Fan et al., 2006; Wang et al., 2021). The volcanic rocks in northern Hainan Island display the widest age span, ranging from 34.78 Ma to 0.013 Ma. In contrast, the volcanic rocks in the southern LP range from 12.46 Ma to 0.48 Ma, while those in the northern LP range from 11.51 Ma to 0.1 Ma. The shortest age span is observed on Weizhou Island, where volcanic rocks date from 1.42 Ma to 0.036 Ma. This distribution suggests that volcanic activity of LQA has persisted into modern times, with the earliest activity beginning in the southern region and gradually progressing toward the northwest.

The earlier onset and longer duration of volcanic activity in northern Hainan Island are likely due to the mantle plume. In contrast, the southern LP, northern LP, and Weizhou Island, being relatively further from the plume's core, experienced volcanic activity later as magma migrated through distal branches of the plume (Figure 1). This spatial and temporal pattern may indicate that the initial phase of volcanism was driven by lithospheric thinning due to tectonic extension, while later phases were predominantly influenced by upwelling of the Hainan mantle plume. The progressive northward expand of volcanic activity concurs with the hypothesis that magma generation and eruption were increasingly controlled by the mantle plume as tectonic influences related to the SCS extension diminished (Xie et al., 2023). This transition from tectonically-driven to plume-dominated volcanism

TABLE 5 Age data set of volcanic rocks in the LQA.

Sample id	Site	Detailed location	Age (Ma)	Methods	References
NZ-12	NLP	South Nayan Beach	3.6	K-Ar	This study
NZ-22	NLP	North Nayan Beach	1.11	K-Ar	
NZ-28	NLP	North Nayan Beach	1.04	K-Ar	
81-H-15	NHI	Jinniu Ridge	16.77	K-Ar	Zhu and Wang (1989)
81-H-16	NHI	ZK1	16.04	K-Ar	
81-H-13	NHI	Jinniu Ridge	11.68	K-Ar	
81-H-14	NHI	ZK1	6.62	Ar-Ar	
81-H-3	NHI	Niumu Ridge	5.34	K-Ar	
81-H-18	NHI	Qiongshan	5.08	K-Ar	
81-H-26	NHI	Jinji Ridge, Dinan	4.11	K-Ar	
81-H-1	NHI	Luyuan Village, Penglai	4.05	K-Ar	
81-H-24	NHI	Fu Mountain, Chengmai	1.93	K-Ar	
81-H-22	NHI	Bochang	1.65	K-Ar	
81-H-25	NHI	Fu Mountain, Chengmai	1.64	K-Ar	
81-H-20	NHI	Lingkou	1.45	K-Ar	
81-K-21	SLP	Hole 275	12.46	K-Ar	
81-K-11	SLP	Stone Ridge	6.12	K-Ar	
81-K-38	SLP	Hole 725	5.62	K-Ar	
81-K-4	SLP	Western Xingfu Farm	3.61	K-Ar	
81-K-10	SLP	Eastern Nanhua Farm	3.09	K-Ar	
81-K-12	SLP	Haian Port	3.04	K-Ar	
81-K-18	SLP	Hole 275	2.96	K-Ar	
81-K-2	SLP	Wushi Port	2.28	K-Ar	
81-K-15	SLP	Bijia Mountain	1.05	K-Ar	
81-K-31	SLP	Hole 722 in Yongshi Farm	1.05	K-Ar	
GS2-1	WZ	Weizhou Island	1.42–0.49	Stratigraphy	Zhang et al. (2020)
GS4-1	WZ	Weizhou Island	1.42–0.49	Stratigraphy	
GS5-1	WZ	Weizhou Island	1.42–0.49	Stratigraphy	
GS5-2	WZ	Weizhou Island	1.42–0.49	Stratigraphy	
GS6-1	WZ	Weizhou Island	1.42–0.49	Stratigraphy	
GS6-2	WZ	Weizhou Island	1.42–0.49	Stratigraphy	
WZ-1	WZ	Weizhou Island	1.42–0.49	Stratigraphy	

(Continued on the following page)

TABLE 5 (*Continued*) Age data set of volcanic rocks in the LQA.

Sample id	Site*	Detailed location	Age (Ma)	Methods	References
-	NHI	Jinniu Ridge, Haikou	3.82	K-Ar	Huang et al. (1993)
-	NHI	Meixia Coast, Lingao	0.73	K-Ar	
-	NHI	Wenge Lake, Wenchang	0.6263	K-Ar	
-	NHI	Eman Ridge	0.21	K-Ar	
-	NHI	Changliu, Haikou	0.0983	K-Ar	
-	NLP	Longshui Ridge, Donghai Island	0.1125	K-Ar	
-	NLP	Longshui Ridge, Donghai Island	0.1	K-Ar	
-	SLP	Tianxi, Xuwen	2.05	K-Ar	
-	SLP	Youhao Farm, Xuwen	1.579	K-Ar	
-	SLP	Yongshi Farm, Xuwen	1.11	K-Ar	
-	SLP	Youhao Farm, Xuwen	0.8374	K-Ar	
HSL-1	NHI	Heishan ridge	5.3–2.58	Stratigraphy	Wang et al. (2021)
HSL-4	NHI	Heishan ridge	5.3–2.58	Stratigraphy	
HSL-5	NHI	Heishan ridge	5.3–2.58	Stratigraphy	
HSL-6	NHI	Heishan ridge	5.3–2.58	Stratigraphy	
CTC1-1	NHI	Chitu Village	2.58–0.77	Stratigraphy	
CTC1-2	NHI	Chitu Village	2.58–0.77	Stratigraphy	
CTC1-4	NHI	Chitu Village	2.58–0.77	Stratigraphy	
CTC2-1	NHI	Chitu Village	2.58–0.77	Stratigraphy	
CTC2-4	NHI	Chitu Village	2.58–0.77	Stratigraphy	
CTC2-5	NHI	Chitu Village	2.58–0.77	Stratigraphy	
LHL-1	NHI	Leihu ridge	0.01	Stratigraphy	
LHL-2	NHI	Leihu ridge	0.01	Stratigraphy	
LHL-5	NHI	Leihu ridge	0.01	Stratigraphy	
YX-1	NHI	Yongxing	0.01	Stratigraphy	
YX-3	NHI	Yongxing	0.01	Stratigraphy	
YX-4	NHI	Yongxing	0.01	Stratigraphy	
YX-5	NHI	Yongxing	0.01	Stratigraphy	
-	SLP	Tianyang, Xuwen	0.4775	K-Ar	Chen (1990)
-	NHI	Fu Mountain, Chengmai	34.78	K-Ar	Feng (1992)
-	NHI	Duowen Ridge, Lingao	8.97	K-Ar	
-	NHI	Xiuying village, Haikou	6.27	K-Ar	
-	NHI	Yongxing, Qiong Mountain	5.19	K-Ar	

(Continued on the following page)

TABLE 5 (*Continued*) Age data set of volcanic rocks in the LQA.

Sample id	Site*	Detailed location	Age (Ma)	Methods	References
-	NHI	Yongxing, Qiong Mountain	4.26	K-Ar	
-	NHI	Lingbei, Suixi	2.8	K-Ar	
-	NHI	Lingbei, Suixi	2.1	K-Ar	
-	NHI	Jinniu Ridge, Haikou	2	K-Ar	
-	NHI	Fu Mountain, Chengmai	0.99	K-Ar	
-	NHI	Yanzhi village, Qiong Mountain	0.83	K-Ar	
-	NHI	Deyi Ridge, Danzhou	0.64	K-Ar	
-	NHI	Ding village, Qiongshan	0.35	K-Ar	
-	NHI	Miao Ridge, Wenchang	0.21	K-Ar	
-	NHI	Leihu ridge	0.013	K-Ar	
-	NLP	Huguangyan, Zhanjing	0.127	K-Ar	
-	SLP	Yongshi Farm, Xuwen	6.31	K-Ar	
-	SLP	Yongshi Farm, Xuwen	2.9	K-Ar	
-	SLP	Qianlong Ridge, Xuwen	2.68	K-Ar	
-	SLP	Yongshi Farm, Xuwen	1.7	K-Ar	
-	SLP	Yongshi Farm, Xuwen	1.2	K-Ar	
-	SLP	Yongshi Farm, Xuwen	0.85	K-Ar	
-	WZ	Eastern Weizhou Island	1.26	K-Ar	
-	NHI	Mutang, Danzhou	28.4348	K-Ar	Sun (1991)
-	NHI	Penglai, Wenchang	11.829	K-Ar	
-	NHI	Penglai, Wenchang	6.9222	K-Ar	
-	NHI	Wenke village, Qiong Mountain	5.5543	K-Ar	
-	NHI	Rongtang village, Qiong Mountain	3.8072	K-Ar	
-	NHI	Penglai, Wenchang	2.7415	K-Ar	
-	NHI	Huangzhu, Dinan	1.3158	K-Ar	
-	NLP	Lingbei, Suixi	11.5107	K-Ar	
-	NLP	Lingbei, Suixi	0.9043	K-Ar	
-	SLP	Huoju Farm, Haikang	2.3002	K-Ar	
-	SLP	Tianyang, Xuwen	1.8799	K-Ar	
2–2	NHI	Hainan	5.3–2.58	Stratigraphic	Zhao et al. (2021)
3–1	NHI	Hainan	5.3–2.58	Stratigraphic	
4–8	NHI	Hainan	5.3–2.58	Stratigraphic	
5–1	NHI	Hainan	5.3–2.58	Stratigraphic	

(Continued on the following page)

TABLE 5 (*Continued*) Age data set of volcanic rocks in the LQA.

Sample id	Site*	Detailed location	Age (Ma)	Methods	References
7–6	NHI	Hainan	5.3–2.58	Stratigraphic	
11–8	NHI	Hainan	5.3–2.58	Stratigraphic	
14–1	NHI	Hainan	5.3–2.58	Stratigraphic	
16–1	NHI	Hainan	5.3–2.58	Stratigraphic	
17–1	NHI	Hainan	5.3–2.58	Stratigraphic	
22–1	NLP	Leizhou	1.8–0.7	Stratigraphic	
23–2	NLP	Leizhou	1.8–0.7	Stratigraphic	
19–1	SLP	Leizhou	1.8–0.7	Stratigraphic	
19–3	SLP	Leizhou	1.8–0.7	Stratigraphic	
20–8	SLP	Leizhou	1.8–0.7	Stratigraphic	
19–4	SLP	Leizhou	1.8–0.7	Stratigraphic	
20–3	SLP	Leizhou	1.8–0.7	Stratigraphic	
20–4	SLP	Leizhou	1.8–0.7	Stratigraphic	
20–9	SLP	Leizhou	1.8–0.7	Stratigraphic	
20–10	SLP	Leizhou	1.8–0.7	Stratigraphic	
18–1	SLP	Leizhou	1.8–0.7	Stratigraphic	
03WZ-08	WZ	Intertidal zone north of the Hengling Mountains	0.49	K-Ar	Fan et al. (2006)
04WZ-12	WZ	Xieyang village	0.57	K-Ar	
03WZ-19	WZ	West Cape intertidal zone	0.58	K-Ar	
03WZ-13	WZ	channel marking tower	0.59	K-Ar	
04WZ-07	WZ	Guogai Ridge	0.6	K-Ar	
04WZ-21	WZ	North Harbour intertidal zone	0.75	K-Ar	
04WZ-06	WZ	Guogai Ridge	0.79	K-Ar	
03WZ-12	WZ	Lower part of the crocodile mouth erosion platform	0.86	K-Ar	
03WZ-14	WZ	Eastern Shangshilokou Village	1.42	K-Ar	
06WZ-BK	WZ	Shells from the Xieyang Island Accumulation	0.036	^{14}C	

provides crucial insights into the geological evolution of the LQA and the underlying mechanisms driving volcanic activity across the region.

5.3 Interaction between Hainan mantle plume and paleo-subducted slab

Previous studies have shown that the volcanic rocks in the LQA are predominantly of the OIB type with certain IAB type, mainly originating from the Hainan mantle plume or as a result of mixing between mantle plume materials and ancient subducted slab components (Ho et al., 2000; Zou and Fan, 2010; Zhang et al., 2020; Zhao et al., 2021). Geochemical analyses indicate that the volcanic rocks in the LQA predominantly exhibit OIB characteristics, reflecting the pivotal role of the mantle plume in controlling the chemical composition and eruption patterns of the magma. Sr-Nd-Pb-Hf isotope data further reveal that the mantle source of these volcanic rocks reflects the geochemical heterogeneity of a mantle plume, with isotopic characteristics

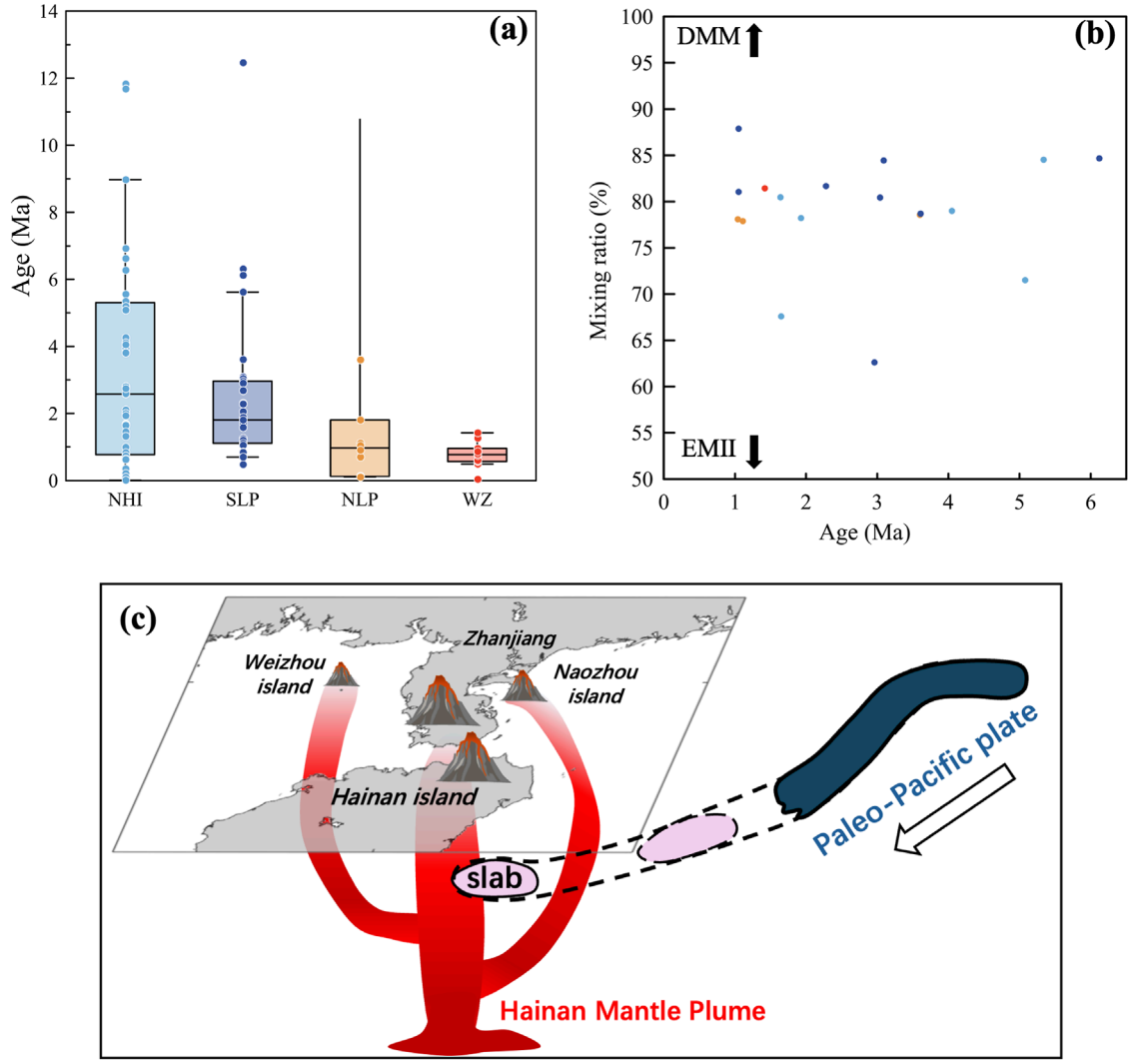

FIGURE 10
(a) All type age data set of volcanic rocks in the LQA (Huang et al., 1993; Zhu and Wang, 1989; Zhang et al., 2020; Fan et al., 2006; Wang et al., 2021). The boxes indicate the range between the first (25%) and the third (75%) quantiles. The solid lines in the boxes indicate the median. The two caps indicate the age data of 10%–90% range; **(b)** DMM-EMII mixing end-member proportions derived from Sr-Nd isotope calculations versus K-Ar ages (Huang et al., 1993; Zhu and Wang, 1989; Zhang et al., 2020; Wang et al., 2012; Zhao et al., 2021; Fan et al., 2008; Li et al., 2014); **(c)** Schematic diagram of slab and Hainan Mantle Plume mixing (Li et al., 2018; Xia et al., 2016).

commonly associated with DMM and EMII signatures observed across nearly entire study areas (Ho et al., 2000; Zou and Fan, 2010; Zhang et al., 2020; Zhao et al., 2021). Based on the linear mixing model of DMM and EMII end-members calculated from the $^{87}Sr/^{86}Sr$-$^{143}Nd/^{144}Nd$ isotopic diagram, combined with K-Ar geochronological data (Figure 10B), it is shown that since 6 Ma, the contribution of the EMII to the source of Cenozoic volcanic rocks in the LQA has increased. A possible mechanism is the progressive upwelling of the mantle plume, which leads to an enrichment of the EMII component. Another possibility is the incorporation of residual Mesozoic subducted slabs during the upwelling process, allowing recycled materials to enter the mantle and occupy a larger proportion in the magma source region.

The temporal and spatial distribution characteristics of volcanic rocks in the region provide new insights into the possible mechanisms of ancient subduction zones' involvement in magmatic activities. Temporally, volcanic activity in the region initiated earlier in the south and progressively became active toward the north. The volcanic rocks on Weizhou Island, located west of the same latitude as northern LP, are generally younger, while volcanic activity in the southern LP occurred earlier than the northern LP, with northern Hainan Island showing the earliest volcanic activity. This temporal difference is closely related to the spatial distribution pattern. The Hainan mantle plume is generally believed to be located in northeast of Hainan Island, which suggests that volcanic activity in northeastern Hainan Island, being closer to the core of the

plume, occurred earlier, while Weizhou Island and northern LP, being relatively farther from the plume, experienced later volcanic activity. This trend is consistent with the position of the Hainan mantle plume (Toyokuni et al., 2022; Xia et al., 2016; Lei et al., 2009; Lebedev and Nolet, 2003; Chen et al., 2021; Hua et al., 2022).

The volcanic rocks in the southern LP, as well as northern Hainan Island, display characteristics of OIB, IAB and OIB-IAB transition types (Zhang et al., 2020; Yung-Tan et al., 2022; An et al., 2017; Wang et al., 2012; Zhao et al., 2021; Chen et al., 2023), which differ from the typical OIB rocks associated with mantle plumes. Previous studies suggested that the mantle source regions in these areas were not only influenced by the mantle plume but also possibly mixed with recycled materials from ancient subducted slabs (Zhang et al., 2020; Yung-Tan et al., 2022; An et al., 2017; Wang et al., 2012; Zhao et al., 2021; Chen et al., 2023). This hypothesis is further supported by our combined isotopic data, particularly in Sr-Nd and Pb isotope diagrams, where samples from southern LP and northern Hainan Island show greater dispersion (Figures 5, 6), indicating that the mantle source regions in these areas may have undergone complex mixing processes. However, the Naozhou Island located in northern LP (this study) and the Weizhou Island located in western LP (Zhang et al., 2020) merely show OIB type basalts which may indicate deriving from the Hainan mantle plume rather than paleo-subducted slab. This distribution can be explained by the branched Hainan mantle plume model suggested by Xia et al. (Xia et al., 2016) and concurs with the subduction direction of the Late Mesozoic subduction zone along the northern SCS margin, which trends approximately from southeast to northwest (Li et al., 2018), implying that the influence of ancient subducted slab materials focused on the center location of the Hainan mantle plume merely (Figure 10C).

6 Conclusion

This study conducted K-Ar dating on basalt samples from Naozhou Island, revealing two periods of volcanic activities: approximately 3.6 Ma (late Pliocene) and 1 Ma (Pleistocene), providing a refined temporal framework for volcanic activity on the island. The basalts on Naozhou Island have undergone limited crustal contamination but intermediate fractional crystallization. Geochemical and isotopic analyses indicate that the volcanic rocks on Naozhou Island are of the OIB-type, primarily derive from a mixture of DMM and EMII, may originate from the Hainan mantle plume. By integrating data from other volcanic rocks in the LQA, this study further elucidates the temporal and spatial evolution of volcanic activity across the entire LQA region. The results demonstrate that the Hainan mantle plume is the primary driver of magmatic activity in the LQA. Moreover, isotopic analysis across different regions reveals dispersion, particularly in southern LP and northern Hainan Island, coupled with the presence of IAB and OIB-IAB transitional characteristics, suggests a significant role of recycled subducted slab material may participate in the magma source. However, the Naozhou Island located in northern LP and the Weizhou Island located in western LP merely show OIB type basalts which may indicate deriving from the branched Hainan mantle plume rather than paleo-subducted slab. The spatial distribution feature of the interaction between branched Hainan Mantle Plume and paleo-subducted slab is in accord with the subduction direction of the Late Mesozoic subduction zone along the northern margin of the SCS.

Data availability statement

The datasets presented in this study can be found in online repositories. The names of the repository/repositories and accession number(s) can be found in the article/Supplementary Material.

Author contributions

JX: Conceptualization, Data curation, Formal Analysis, Investigation, Methodology, Software, Visualization, Writing–original draft, Writing–review and editing. HX: Conceptualization, Funding acquisition, Investigation, Project administration, Resources, Supervision, Validation, Writing–review and editing. ZL: Investigation, Methodology, Writing–original draft. YC: Formal Analysis, Investigation, Methodology, Visualization, Writing–review and editing. HS: Funding acquisition, Investigation, Resources, Supervision, Validation, Writing–review and editing.

Funding

The author(s) declare that financial support was received for the research, authorship, and/or publication of this article. This work was jointly supported by Key Laboratory of Marine Mineral Resources, Ministry of Natural Resources, Guangzhou (No.KLMMR-2024-K02), Guangdong Basic and Applied Basic Research Foundation (No. 2023A1515030124), Program for Scientific Research Start-up Funds of Guangdong Ocean University (No. E15173), Marine Science Research Team Project of Guangdong Ocean University (No. 002026002004), Guangdong Provincial College Innovation Team Project (2019KCXTF021), and First-class Discipline Plan of Guangdong Province (080503032101).

Acknowledgments

The authors would like to express sincere gratitude to the editor and reviewers for their insightful suggestions and constructive feedback, which have significantly contributed to the improvement and refinement of this manuscript, and to Yongyi Luo, Lihui

Wang, and Zhiyong Deng for their participation in the field work.

Conflict of interest

The authors declare that the research was conducted in the absence of any commercial or financial relationships that could be construed as a potential conflict.

Generative AI statement

The authors declare that no Generative AI was used in the creation of this manuscript.

Publisher's note

Supplementary material

The Supplementary Material for this article can be found online at: https://www.frontiersin.org/articles/10.3389/feart.2025.1532124/full#supplementary-material

References

An, A. R., Choi, S. H., Yu, Y., and Lee, D.-C. (2017). Petrogenesis of late cenozoic basaltic rocks from southern Vietnam. *Lithos* 272-273, 192–204. doi:10.1016/j.lithos.2016.12.008

Briais, A., Patriat, P., and Tapponnier, P. (2012). Updated interpretation of magnetic anomalies and seafloor spreading stages in the south China Sea: implications for the Tertiary tectonics of Southeast Asia. *J. Geophys. Res. Solid Earth* 98 (B4), 6299–6328. doi:10.1029/92jb02280

Chang, S. J., Ferreira, A. M., and Faccenda, M. (2016). Upper- and mid-mantle interaction between the Samoan plume and the Tonga-Kermadec slabs. *Nat. Commun.* 7, 10799. doi:10.1038/ncomms10799

Chen, J. (1990). *Quaternary Geology of Tianyang volcanic lake, Guangdong*. Beijing: Geology Pres.

Chen, S.-S., Gao, R., Wang, Z., Hou, T., Liao, J., Yan, C., et al. (2021). Coexistence of Hainan plume and stagnant slab in the mantle transition zone beneath the southSouth China sea spreading ridge: constraints from volcanic glasses and seismic tomography. *Lithosphere* 2021 (Special 2). doi:10.2113/2021/6619463

Chen, S.-S., Wu, D.-Y., Gao, R., Cheng, Q., and Liu, J.-Q. (2023). *In-situ* Sr isotope disequilibrium in plagioclases from Late Cenozoic basalts in Leiqiong area: evidence for the role of the Hainan plume and mantle metasomatism due to a paleo-subduction event. *Front. Earth Sci.* 11. doi:10.3389/feart.2023.1090803

Choi, S. H., and Mukasa, S. B. (2012). Lu–Hf and Sm–Nd isotope systematics of Korean spinel peridotites: a case for metasomatically induced Nd–Hf decoupling. *Lithos* 154, 263–276. doi:10.1016/j.lithos.2012.07.017

Cui, Y., Shao, L., Li, Z.-X., Zhu, W., Qiao, P., and Zhang, X. (2021). A Mesozoic Andean-type active continental margin along coastal South China: new geological records from the basement of the northern South China Sea. *Gondwana Res.* 99, 36–52. doi:10.1016/j.gr.2021.06.021

Dai, L.-Q., Zheng, F., Zhao, Z.-F., and Zheng, Y.-F. (2018). Geochemical insights into the lithology of mantle sources for Cenozoic alkali basalts in West Qinling, China. *Lithos* 302-303, 86–98. doi:10.1016/j.lithos.2017.12.013

Dalziel, I. W. D., Lawver, L. A., and Murphy, J. B. (2000). Plumes, orogenesis, and supercontinental fragmentation. *Earth Planet. Sci. Lett.* 178 (1-2), 1–11. doi:10.1016/s0012-821x(00)00061-3

Druken, K. A., Kincaid, C., Griffiths, R. W., Stegman, D. R., and Hart, S. R. (2014). Plume–slab interaction: the Samoa–Tonga system. *Phys. Earth Planet. Interiors* 232, 1–14. doi:10.1016/j.pepi.2014.03.003

Dupré, B., and Allègre, C. J. (1983). Pb–Sr isotope variation in Indian Ocean basalts and mixing phenomena. *Nature* 303 (5913), 142–146. doi:10.1038/303142a0

Fan, Q., Sun, Q., Long, A., Yin, K., Sui, J., Li, N., et al. (2006). Geology and eruption history of volcanoes in Weizhou island and Xieyang island, northern Bay (in Chinese). *Acta Petrol. Sin.* 6 (22), 1529–1537. doi:10.3321/j.issn:1000-0569.2006.06.011

Fan, Q., Sun, Q., Sui, J., and Li, N. (2008). Trace-element and isotopic geochemistry of volcanic rocks and it's techtonic implications in Weizhou Island and Xieyang Island, Northern Bay (in Chinese). *Acta Petrol. Sin.* 6 (24), 1323–1332.

Feng, G. (1992). Basic characteristics and relationship to tectonic environment of the Late Cenozoic basalts along the coast of South China Sea (in Chinese). *Suppl. J. Sunyatsen Univ.* 1 (12), 93–103.

Flower, M. F. J., Zhang, M., Chen, C.-Y., Tu, K., and Xie, G. (1992). Magmatism in the southSouth China basin. *Chem. Geol.* 97 (1-2), 65–87. doi:10.1016/0009-2541(92)90136-s

Foulger, G. R., and Natland, J. H. (2003). Geology. Is "hotspot" volcanism a consequence of plate tectonics? *Science* 300 (5621), 921–922. doi:10.1126/science.1083376

Gazel, E., Hoernle, K., Carr, M. J., Herzberg, C., Saginor, I., den Bogaard, P. V., et al. (2011). Plume–subduction interaction in southern Central America: mantle upwelling and slab melting. *Lithos* 121 (1-4), 117–134. doi:10.1016/j.lithos.2010.10.008

Gorbatov, A., Fukao, Y., Widiyantoro, S., and Gordeev, E. (2001). Seismic evidence for a mantle plume oceanwards of the Kamchatka-Aleutian trench junction. *Geophys. J. Int.* 146 (2), 282–288. doi:10.1046/j.0956-540x.2001.01439.x

Hamelin, B., and Allègre, C. J. (1985). Large-scale regional units in the depleted upper mantle revealed by an isotope study of the South-West Indian Ridge. *Nature* 315 (6016), 196–199. doi:10.1038/315196a0

Hart, S. R. (1984). A large-scale isotope anomaly in the Southern Hemisphere mantle. *Nature* 309 (5971), 753–757. doi:10.1038/309753a0

Ho, K.-s., Chen, J.-c., and Juang, W.-s. (2000). Geochronology and geochemistry of late Cenozoic basalts from the Leiqiong area, southern China. *J. Asian Earth Sci.* 18 (3), 307–324. doi:10.1016/s1367-9120(99)00059-0

Hoang, N., Flower, M. F. J., and Carlson, R. W. (1996). Major, trace element, and isotopic compositions of Vietnamese basalts: interaction of hydrous EM1-rich asthenosphere with thinned Eurasian lithosphere. *Geochimica Cosmochimica Acta* 60 (22), 4329–4351. doi:10.1016/s0016-7037(96)00247-5

Hoàng, N., Flower, M. F. J., Ctọn, C., Xuân, P. T., Quý, H. V., and Sơn, T. T. (2013). Collision-induced basalt eruptions at Pleiku and Buôn Mê Thuột, south-central Viet Nam. *J. Geodyn.* 69, 65–83. doi:10.1016/j.jog.2012.03.012

Hofmann, A. W. (1997). Mantle geochemistry: the message from oceanic volcanism. *Nature* 385 (6613), 219–229. doi:10.1038/385219a0

Hua, Y., Zhao, D., and Xu, Y. G. (2022). Azimuthal anisotropy tomography of the Southeast Asia subduction system. *J. Geophys. Res. Solid Earth* 127 (2). doi:10.1029/2021jb022854

Huang, Z., Cai, F., Han, Z., Chen, J., Zong, Y., and Lin, X. (1993). *Leiqiong quaternary volcano*. Beijing: Science Press.

Kincaid, C., Druken, K. A., Griffiths, R. W., and Stegman, D. R. (2013). Bifurcation of the Yellowstone plume driven by subduction-induced mantle flow. *Nat. Geosci.* 6 (5), 395–399. doi:10.1038/ngeo1774

Lebedev, S., and Nolet, G. (2003). Upper mantle beneath Southeast Asia from S velocity tomography. *J. Geophys. Res. Solid Earth* 108 (B1). doi:10.1029/2000jb000073

Lei, J., Zhao, D., Steinberger, B., Wu, B., Shen, F., and Li, Z. (2009). New seismic constraints on the upper mantle structure of the Hainan plume. *Phys. Earth Planet. Interiors* 173 (1-2), 33–50. doi:10.1016/j.pepi.2008.10.013

Le Maitre, R. W., Streckeisen, A., Zanettin, B., Le Bas, M. J., Bonin, B., and Bateman, P. (2002). Igneous Rocks.

Li, C. F., Li, J., Ding, W., Franke, D., Yao, Y., Shi, H., et al. (2015). Seismic stratigraphy of the central South China Sea basin and implications for neotectonics. *J. Geophys. Res. Solid Earth* 120 (3), 1377–1399. doi:10.1002/2014jb011686

Li, F., Sun, Z., and Yang, H. (2018). Possible spatial distribution of the Mesozoic volcanic arc in the present-day South China sea continental margin and its tectonic implications. *J. Geophys. Res. Solid Earth* 123 (8), 6215–6235. doi:10.1029/2017jb014861

Li, N., Yan, Q., Chen, Z., and Shi, X. (2014). Geochemistry and petrogenesis of Quaternary volcanism from the islets in the eastern Beibu Gulf: evidence for Hainan plume. *Acta Oceanol. Sin.* 32 (12), 40–49. doi:10.1007/s13131-013-0386-1

Li, Z.-X., and Li, X.-H. (2007). Formation of the 1300-km-wide intracontinental orogen and postorogenic magmatic province in Mesozoic South China: a flat-slab subduction model. *Geology* 35 (2), 179. doi:10.1130/g23193a.1

Liu, J.-Q., Ren, Z.-Y., Nichols, A. R. L., Song, M.-S., Qian, S.-P., Zhang, Y., et al. (2015). Petrogenesis of late cenozoic basalts from North Hainan island: constraints from melt inclusions and their host olivines. *Geochimica Cosmochimica Acta* 152, 89–121. doi:10.1016/j.gca.2014.12.023

Mahoney, J. J., Natland, J. H., White, W. M., Poreda, R., Bloomer, S. H., Fisher, R. L., et al. (2012). Isotopic and geochemical provinces of the western Indian ocean spreading centers. *J. Geophys. Res. Solid Earth* 94 (B4), 4033–4052. doi:10.1029/jb094ib04p04033

Mériaux, C. A., Duarte, J. C., Schellart, W. P., and Mériaux, A. S. (2015). A two-way interaction between the Hainan plume and the Manila subduction zone. *Geophys. Res. Lett.* 42 (14), 5796–5802. doi:10.1002/2015gl064313

Mériaux, C. A., Mériaux, A. S., Schellart, W. P., Duarte, J. C., Duarte, S. S., and Chen, Z. (2016). Mantle plumes in the vicinity of subduction zones. *Earth Planet. Sci. Lett.* 454, 166–177. doi:10.1016/j.epsl.2016.09.001

Niu, Y., and O'Hara, M. J. (2003). Origin of ocean island basalts: a new perspective from petrology, geochemistry, and mineral physics considerations. *J. Geophys. Res. Solid Earth* 108 (B4). doi:10.1029/2002jb002048

Obrebski, M., Allen, R. M., Xue, M., and Hung, S. H. (2010). Slab-plume interaction beneath the Pacific northwest. *Geophys. Res. Lett.* 37 (14). doi:10.1029/2010gl043489

Plank, T., and Langmuir, C. H. (1998). The chemical composition of subducting sediment and its consequences for the crust and mantle. *Chem. Geol.* 145 (3-4), 325–394. doi:10.1016/s0009-2541(97)00150-2

Price, A. A., Jackson, M. G., Blichert-Toft, J., Hall, P. S., Sinton, J. M., Kurz, M. D., et al. (2014). Evidence for a broadly distributed Samoan-plume signature in the northern Lau and North Fiji Basins. *Geochem. Geophys. Geosystems* 15 (4), 986–1008. doi:10.1002/2013gc005061

Rudnick, R. L., and Gao, S. (2003). Composition of the continental crust. *Treatise Geochem.* 3, 1–64. doi:10.1016/b0-08-043751-6/03016-4

Salters, V. J. M., and Stracke, A. (2004). Composition of the depleted mantle. *Geochem. Geophys. Geosystems* 5 (5). doi:10.1029/2003gc000597

Smith, R. B., Jordan, M., Steinberger, B., Puskas, C. M., Farrell, J., Waite, G. P., et al. (2009). Geodynamics of the Yellowstone hotspot and mantle plume: seismic and GPS imaging, kinematics, and mantle flow. *J. Volcanol. Geotherm. Res.* 188 (1-3), 26–56. doi:10.1016/j.jvolgeores.2009.08.020

Staudigel, H., Zindler, A., Hart, S. R., Leslie, T., Chen, C. Y., and Clague, D. (1984). The isotope systematics of a juvenile intraplate volcano: Pb, Nd, and Sr isotope ratios of basalts from Loihi Seamount, Hawaii. *Earth Planet. Sci. Lett.* 69 (1), 13–29. doi:10.1016/0012-821x(84)90071-2

Steiger, R. H., and Jäger, E. (1977). Subcommission on geochronology: convention on the use of decay constants in geo- and cosmochronology. *Earth Planet. Sci. Lett.* 36 (3), 359–362. doi:10.1016/0012-821x(77)90060-7

Sun, J. (1991). Cenozoic volcanic activity in the northern South China Sea and Guangdong coastal area. *Mar. Geol. and Quat. Geol.* (3), 45–66. doi:10.16562/j.cnki.0256-1492.1991.03.005

Sun, S. S., and McDonough, W. F. (1989). Chemical and isotopic systematics of oceanic basalts: implications for mantle composition and processes. *Geol. Soc. Lond. Spec. Publ.* 42 (1), 313–345. doi:10.1144/gsl.sp.1989.042.01.19

Taylor, B., and Hayes, D. E. (1983). "Origin and history of the South China sea basin," in *The tectonic and geologic evolution of Southeast asian Seas and Islands: Part 2*. Editors D. E. Hayes American Geophysical Union: Washington, D.C.

Toyokuni, G., Zhao, D., and Kurata, K. (2022). Whole-mantle tomography of Southeast Asia: new insight into plumes and slabs. *J. Geophys. Res. Solid Earth* 127 (11). doi:10.1029/2022jb024298

Tu, K., Flower, M. F. J., Carlson, R. W., Zhang, M., and Xie, G. (1991). Sr, Nd, and Pb isotopic compositions of Hainan basalts (south China): implications for a subcontinental lithosphere Dupal source. *Geology* 19 (6), 567. doi:10.1130/0091-7613(1991)019<0567:snapic>2.3.co;2

von Huene, R., Ranero, C. R., and Vannucchi, P. (2004). Generic model of subduction erosion. *Geology* 32 (10), 913. doi:10.1130/g20563.1

Wang, J., Su, Y., Zheng, J., Gao, S., Dai, H., Ping, X., et al. (2019). Geochronology and petrogenesis of Jurassic intraplate alkali basalts in the Junggar terrane, NW China: implication for low-volume basaltic volcanism. *Lithos* 324-325, 202–215. doi:10.1016/j.lithos.2018.11.002

Wang, L., Zhao, Y., Li, N., and Chen, Z. (2023). The genesis of pyroclasts and the mechanism of submarine eruption of Naozhou Island in Guangdong, South China. *Acta Petrol. Sin.* 39 (3), 907–920. doi:10.18654/1000-0569/2023.03.16

Wang, P.-Y., Gu, X.-Y., Kuritani, T., Hanski, E., and Xia, Q.-K. (2021). Highly variable H2O/Ce ratios in the Hainan mantle plume. *Lithos*, 406–407. doi:10.1016/j.lithos.2021.106516

Wang, X.-C., Li, Z.-X., Li, X.-H., Li, J., Liu, Y., Long, W.-G., et al. (2012). Temperature, pressure, and composition of the mantle source region of late Cenozoic basalts in Hainan island, SE Asia: a consequence of a young thermal mantle plume close to subduction zones? *J. Petrology* 53 (1), 177–233. doi:10.1093/petrology/egr061

Wang, X.-C., Li, Z.-X., Li, X.-H., Li, J., Xu, Y.-G., and Li, X.-H. (2013). Identification of an ancient mantle reservoir and young recycled materials in the source region of a young mantle plume: implications for potential linkages between plume and plate tectonics. *Earth Planet. Sci. Lett.* 377-378, 248–259. doi:10.1016/j.epsl.2013.07.003

Wang, X.-J., Chen, L.-H., Hofmann, A. W., Hanyu, T., Kawabata, H., Zhong, Y., et al. (2018). Recycled ancient ghost carbonate in the Pitcairn mantle plume. *Proc. Natl. Acad. Sci.* 115 (35), 8682–8687. doi:10.1073/pnas.1719570115

Weis, D., Kieffer, B., Hanano, D., Nobre Silva, I., Barling, J., Pretorius, W., et al. (2007). Hf isotope compositions of U.S. Geological Survey reference materials. *Geochem. Geophys. Geosystems* 8 (6). doi:10.1029/2006gc001473

Weis, D., Kieffer, B., Maerschalk, C., Barling, J., de Jong, J., Williams, G. A., et al. (2006). High-precision isotopic characterization of USGS reference materials by TIMS and MC-ICP-MS. *Geochem. Geophys. Geosystems* 7 (8). doi:10.1029/2006gc001283

Wendt, J. I., Regelous, M., Collerson, K. D., and Ewart, A. (1997). Evidence for a contribution from two mantle plumes to island-arc lavas from northern Tonga. *Geology* 25 (7), 611. doi:10.1130/0091-7613(1997)025<0611:efacft>2.3.co;2

Wilkinson, J. F. G., and Maitre, R. W. L. (1987). Upper mantle amphiboles and micas and TiO2, K2O, and P2O5 abundances and 100 Mg/Mg+Fe2+Upper mantle amphiboles and micas and TiO2, K2O, and P2O5 abundances and 100 Mg/Mg+Fe2+ ratios of common basalts and andesites: implications for modal mantle metasomatism and undepleted mantle compositions ratios of common basalts and andesites: implications for modal mantle metasomatism and undepleted mantle compositions. *J. Petrology* 28 (1), 37–73. doi:10.1093/petrology/28.1.37

Xia, S., Zhao, D., Sun, J., and Huang, H. (2016). Teleseismic imaging of the mantle beneath southernmost China: new insights into the Hainan plume. *Gondwana Res.* 36, 46–56. doi:10.1016/j.gr.2016.05.003

Xie, H., Qiu, N., Shi, H., Sun, Z., and Zheng, J. (2023). Diachronous basin evolution along northern South China Sea: result of a migrating Hainan plume? *Tectonophysics* 846, 229683. doi:10.1016/j.tecto.2022.229683

Xu, J., Xia, X. P., Lai, C. K., Zhou, M., and Ma, P. (2019). First identification of late permian Nb-enriched basalts in ailaoshan region (SW yunnan, China): contribution from emeishan plume to subduction of eastern paleotethys. *Geophys. Res. Lett.* 46 (5), 2511–2523. doi:10.1029/2018gl081687

Xu, J., Xia, X.-P., Wang, Q., Spencer, C. J., He, B., and Lai, C.-K. (2021). Low-δ18O A-type granites in SW China: evidence for the interaction between the subducted Paleotethyan slab and the Emeishan mantle plume. *GSA Bull.* 134 (1-2), 81–93. doi:10.1130/b35929.1

Xu, Y.-G., Ma, J.-L., Frey, F. A., Feigenson, M. D., and Liu, J.-F. (2005). Role of lithosphere–asthenosphere interaction in the genesis of Quaternary alkali and tholeiitic basalts from Datong, western North China Craton. *Chem. Geol.* 224 (4), 247–271. doi:10.1016/j.chemgeo.2005.08.004

Yan, Q., Castillo, P., Shi, X., Wang, L., Liao, L., and Ren, J. (2015). Geochemistry and petrogenesis of volcanic rocks from Daimao Seamount (South China Sea) and their tectonic implications. *Lithos* 218-219, 117–126. doi:10.1016/j.lithos.2014.12.023

Yan, Q., Shi, X., and Castillo, P. R. (2014). The late Mesozoic–Cenozoic tectonic evolution of the South China Sea: a petrologic perspective. *J. Asian Earth Sci.* 85, 178–201. doi:10.1016/j.jseaes.2014.02.005

Yan, Q., Shi, X., Metcalfe, I., Liu, S., Xu, T., Kornkanitnan, N., et al. (2018). Hainan mantle plume produced late Cenozoic basaltic rocks in Thailand, Southeast Asia. *Sci. Rep.* 8 (1), 2640. doi:10.1038/s41598-018-20712-7

Yan, Q., Shi, X., Wang, K., Bu, W., and Xiao, L. (2008). Major element, trace element, and Sr, Nd and Pb isotope studies of Cenozoic basalts from the South China Sea. *Sci. China Ser. D Earth Sci.* 51 (4), 550–566. doi:10.1007/s11430-008-0026-3

Yang, F., Huang, X.-L., Xu, Y.-G., and He, P.-L. (2023). Bifurcation of mantle plumes by interaction with stagnant slabs in the mantle transition zone: evidence from late Cenozoic basalts within Southeast Asia. *GSA Bull.* doi:10.1130/b36558.1

Yu, X., Liu, Z., Zeng, G., Cao, W., Meas, R., Hoang, L. V., et al. (2022). Mantle plume–stagnant slab interaction controls the generation of a mixed mantle source for continental intraplate basalts. *Lithos*, 426–427. doi:10.1016/j.lithos.2022.106795

Yung-Tan, L., Chou, P.-C., Ho, K.-S., Tsai, Y.-W., and Chang, Y.-J. (2022). Petrogenesis of cenozoic basaltic rocks from the Leiqiong area, South China: evidence from geochemical constraints. *Geochem. Int.* 59 (13), 1199–1234. doi:10.1134/s0016702921130048

Zeng, G., Chen, L. H., Hu, S. L., Xu, X. S., and Yang, L. F. (2013). Genesis of Cenozoic low-Ca alkaline basalts in the Nanjing basaltic field, eastern China: the case for mantle xenolith-magma interaction. *Geochem. Geophys. Geosystems* 14 (5), 1660–1677. doi:10.1002/ggge.20127

Zhang, H. (1990). Basic charcteristics of Cainozoic volcanism in coastal area of South Ching. *J. Disaster Prev. Reduct.* (1), 63–75.

Zhang, H., and Zhao, X. (1984). Characteristics of the neotectonic movement in the hainan island and Leizhou Peninsula area (in Chinese). *Geol. Sci.* 3 (19), 276–287.

Zhang, Y., Yu, K., Fan, T., Yue, Y., Wang, R., Jiang, W., et al. (2020). Geochemistry and petrogenesis of quaternary basalts from Weizhou island, northwestern SouthSouth China sea: evidence for the hainan plume. *Lithos*, 362–363. doi:10.1016/j.lithos.2020.105493

Zhao, Z.-H., Zhang, G.-L., Wang, S., and Zhao, J.-X. (2021). Origin of arc-like intraplate volcanism by melting of lithospheric mantle pyroxenite of the South China continental margin. *Lithos*, 396–397. doi:10.1016/j.lithos.2021.106236

Zhu, B. Q., and Wang, H. F. (1989). Isotopic and chemical evidence for the volcannism with MORB-OIB source characteristics in the Leiqiong area, China (in Chinese). *Geochimica* (3), 193–201. doi:10.3321/j.issn:0379-1726.1989.03.001

Zindler, A., and Hart, S. (1986). Chemical geodynamics. *Annu. Rev. Earth Planet. Sci.* 14 (1), 493–571. doi:10.1146/annurev.earth.14.1.493

Zou, H., and Fan, Q. (2010). U–Th isotopes in Hainan basalts: implications for sub-asthenospheric origin of EM2 mantle endmember and the dynamics of melting beneath Hainan Island. *Lithos* 116 (1-2), 145–152. doi:10.1016/j.lithos.2010.01.010

Zou, H., Zindler, A., Xu, X., and Qi, Q. (2000). Major, trace element, and Nd, Sr and Pb isotope studies of Cenozoic basalts in SE China: mantle sources, regional variations, and tectonic significance. *Chem. Geol.* 171 (1-2), 33–47. doi:10.1016/s0009-2541(00)00243-6